1

2

3

4

Multidecadal Variability and Predictability

of Antarctic Sea Ice in GFDL SPEAR_LO Model

7

8

9

Yushi Morioka[1,2,3], Liping Zhang[2,4], Thomas L. Delworth[2],

Xiaosong Yang[2], Fanrong Zeng[2], Masami Nonaka[1], Swadhin K. Behera[1]

12

1: Application Laboratory, VAiG, JAMSTEC, Yokohama, Kanagawa, Japan
2: Geophysical Fluid Dynamics Laboratory, NOAA, Princeton, New Jersey, USA
3: Atmospheric and Oceanic Sciences Program, Princeton University,
Princeton, New Jersey, USA
4: University Corporation for Atmospheric Research, Boulder, Colorado, USA

18

19

20

21

22

23

Corresponding Author: Yushi Morioka

Showamachi 3173-25, Kanazawa-ku, Yokohama, JAPAN

morioka@jamstec.go.jp, +81-45-778-5509

27

28

The Cryosphere
Discussions

29 **Abstract**

30 Using a state-of-the-art coupled general circulation model, physical processes underlying

31 Antarctic sea ice multidecadal variability and predictability are investigated. Our model

32 simulations constrained with atmospheric reanalysis and observed sea surface temperature

33 broadly capture the observed sea ice extent (SIE) variability with a low sea ice state (late 1970s-

34 1990s) and a high sea ice state (2000s-early 2010s), although the model overestimates the SIE

35 decrease over the Weddell Sea around the 1980s. The low sea ice state is largely due to an

36 occurrence of strong deep convection in the Southern Ocean that subsequently induces

37 anomalous warming of the upper ocean. During the high sea ice period (post-2000s), the deep

38 convection substantially weakens, so that surface wind variability plays greater roles in the SIE

39 variability. Decadal retrospective forecasts started from the above-mentioned constrained

40 model results demonstrate that the Antarctic sea ice multidecadal variability can be skillfully

41 predicted 6-10 years in advance, showing a moderate correlation with the observation (0.4).

42 Ensemble members with a stronger deep convection tend to predict a larger sea ice decrease in

43 the 1980s, whereas the members with a larger surface wind variability tend to predict a larger

44 sea ice increase after the 2000s. Therefore, skillful simulation and prediction of the Antarctic

45 sea ice multidecadal variability require accurate simulation and prediction of both the Southern

46 Ocean deep convection and surface wind variability in the model.

47

48 **Keywords**

49 Antarctic sea ice, Multidecadal variability, Predictability, Coupled general circulation model

50

51

1. Introduction

Antarctic sea ice plays key roles in exchanging heat, momentum, freshwater, and gases between atmosphere and ocean in the Southern Ocean. Formation of sea ice near the Antarctic coast generates high salinity and dense water (e.g., Antarctic Bottom Water; Orsi et al., 1999) that travels into a deeper part of the Southern Ocean and affects global thermohaline circulation. Antarctic sea ice extent (SIE) undergoes substantial seasonal-to-interannual variations (e.g., Yuan and Martinson, 2000; Cavalieri et al., 2003), and shows a slightly increasing trend until 2015 during the satellite era (e.g., Yuan et al., 2017; Parkinson, 2019). This contrasts with a significant SIE decrease in the early and middle twentieth century, estimated from a century-long SIE reconstructed data (Fogt et al., 2022). This implies that a low-frequency variability beyond a decade may exist in the Antarctic SIE. Observation shows that the Antarctic SIE reaches a record high in 2014 but abruptly declines to a record low in late 2016. The Weddell Sea contributes the most to the total sea ice decrease (Turner et al., 2020). The recent Antarctic SIE decrease is attributed to several physical processes, including the upper Southern Ocean warming (Meehl et al., 2019; Zhang et al., 2022b), anomalous warm air advection from the north (Turner et al., 2017) associated with atmospheric teleconnection from the tropics (Wang et al., 2019), and weakening of the midlatitude westerlies (Stuecker et al., 2017; Schlosser et al., 2018) linked to a negative phase of Southern Annual Mode (SAM; Thompson and Wallace, 2000) induced by the weakening of polar stratospheric vortex (Wang et al., 2019). It is still unclear whether the recent SIE decrease is a part of interannual variability or lower-frequency variability (Eayrs et al., 2021).

Most coupled general circulation models (CGCMs) simulate a decreasing trend of the Antarctic SIE in response to both increasing greenhouse gases and stratospheric ozone depletion. The positive SIE trend observed in the past three decades until 2015 cannot be solely explained by anthropogenic forcings, but may be attributed to natural variability (Polvani and Smith, 2013). For example, Goose and Zunz (2014) discussed a role of positive ice-ocean feedback in amplification of sea ice increase using a CGCM control simulation. Once the sea ice starts to increase, the brine released from the sea ice can be transported downward to deeper layers and not incorporated back into the mixed layer. This leads to a decrease in surface salinity, an increase in surface stratification, and thus reduced vertical ocean heat transport, resulting in further increase in sea ice. Lecomte et al. (2017) confirmed this ice-ocean feedback in the Ross Sea using an ocean general circulation model. Even with the climatological wind forcing, the model can simulate a slightly increasing SIE trend associated with the heat loss in the surface mixed layer and the heat gain at the base of the mixed layer.

86   Open-ocean deep convection (Gordon, 1978; Killworth, 1983; Akitomo et al., 1995) in

87   the Southern Ocean is also important for Antarctic sea ice variability. For example, Goosse and

88   Fichefet (2001) examined a role of deep convection in the formation of Weddell polynya (i.e.,

89   open water area enclosed by sea ice) using an ocean-ice model. They found that surface salinity

90   increase owing to brine release during sea ice formation period tends to induce deep convection

91   and entrain the relatively warm water from the subsurface ocean to the surface mixed layer,

92   responsible for sea ice decrease. The link between Weddell polynya and open-ocean deep

93   convection is widely discussed in observational and modeling studies (e.g., Gordon et al., 2007;

94   Cheon et al., 2014, 2015). Recently, Zhang et al. (2019) pointed out that the observed SST

95   cooling and sea ice increasing trends in the Ross and Weddell Seas can be reproduced in the

96   CGCM where they start the simulations from an active phase of the deep convection.

97   On the other hand, surface wind variability also contributes to Antarctic sea ice

98   variability. Turner et al. (2016) attributed the positive SIE trend in the Ross Sea to stronger

99   southerly winds associated with a deepening of the Amundsen Sea Low, which are linked to a

100   negative phase of the Interdecadal Pacific Oscillation (IPO; Power et al., 1999, Meehl et al.,

101   2016) and a positive phase of the Atlantic Multidecadal Oscillation (AMO; Li et al., 2014).

102   The stronger southerly winds tend to enhance northward sea ice advection and increase sea ice

103   concentration in the Ross Sea (Holland and Kwok, 2012). Using a CGCM constrained with

104   atmospheric reanalysis surface winds and observed SST, Blanchard-Wrigglesworth et al.

105   (2021) confirmed the influences of surface winds and SST in the Southern Ocean onto the

106   Antarctic SIE trend and variability. However, their simulations could not well reproduce the

107   low sea ice state in the 1980s and the increasing SIE trend afterwards. Sun and Eisenman (2021)

108   modified the simulations by replacing the model sea ice velocity with the observed sea ice

109   motion and found that their new simulations can capture the Antarctic sea ice increasing trend

110   from 1992 to 2015. The failure of the model in simulating the increasing sea ice trend may be

111   due to the model biases in the sea ice drift velocity.

112   Several studies have reported skillful predictions of regional and pan-Antarctic SIE

113   variability at seasonal-to-interannual timescales (Guemas et al., 2014, 2016; Marchi et al.,

114   2019; Morioka et al., 2019, 2021; Bushuk et al., 2021), and prediction skills of summertime

115   sea ice are generally lower than those of wintertime sea ice. However, few studies have

116   examined the multi-year to decadal sea ice predictability of the Antarctic SIE. Yang et al.

117   (2016) provided broad assessment of the Antarctic SIE predictability using decadal hindcasts

118   from eleven Coupled Model Intercomparison Project Phase 5 (CMIP5) models. They

119   concluded that most of the CMIP5 models do not show promising prediction skills for the

120   Antarctic SIE anomalies. The prediction skills are much lower than the persistence prediction

121   using the observed SIE anomalies. The low prediction skills are likely because most of the

122   models are initialized on every 1 January when the sea ice extent is very low and little sea ice

123   information persists in the models. Most of the models cannot predict the increasing Antarctic

124   SIE trend in the past three decades. When a linear trend is removed from the SIE anomalies,

125   the prediction skills become higher in the Ross Sea and the Weddell Sea. The prediction skills

126   in the initialized hindcasts tend to be higher than those in the uninitialized hindcasts. These

127   results are consistent with a former study (Zunz et al., 2015) that showed skillful prediction of

128   the multi-year Antarctic SIE variability by initializing the model surface air temperature.

129   Recently, Morioka et al. (2022) demonstrated that ocean and sea ice initializations in their

130   CGCM improve decadal sea ice prediction skills in the west Antarctic Seas. They discussed

131   the improvement of prediction skills for the regional sea ice, in particular after 2005 when the

132   subsurface ocean observations increased. However, the model could not capture the sea ice

133   decrease in the 1980s, so we need further efforts to improve our understanding of multidecadal

134   sea ice variability and predictability.

135   In this study, we attempt to address the following two scientific questions: what are

136   relative importance of the Southern Ocean deep convection and the atmospheric variability in

137   the Antarctic SIE multidecadal variability? How far and skillfully can the Antarctic sea ice

138   multidecadal variability be predicted and what are the underlying physical processes? To this

139   end, we examine the Antarctic sea ice multidecadal variability and predictability using the

140   GFDL (Geophysical Fluid Dynamics Laboratory) newly developed Seamless System for

141   Prediction and Earth System Research (SPEAR; Delworth et al., 2020) model. We compare

142   the observation data and model simulations constrained with atmospheric reanalysis surface

143   winds and temperature and observed SST to evaluate how reasonably the model simulates the

144   observed SIE variability. We also clarify the relative importance of atmosphere and ocean in

145   the Antarctic SIE multidecadal variability. Using the decadal retrospective forecasts started

146   from the above constrained model simulations, we attempt to understand to what extent the

147   multidecadal sea ice variability can be skillfully predicted. This paper is organized as follows:

148   Sect. 2 describes observation data and model experiments performed in this study. In Sect. 3,

149   we provide all the observational and model results. In Sect. 4, we put them into the historical

150   context and discuss the remaining issues to be addressed in future work.

151

152   **2. Methodology**

https://doi.org/10.5194/tc-2023-18
Preprint. Discussion started: 28 February 2023
© Author(s) 2023. CC BY 4.0 License.

The Cryosphere
Discussions
Open Access
EGU

2.1. Observation Data

We obtained monthly sea ice concentration (SIC) from the Hadley Centre Global Sea Ice and Sea Surface Temperature version 1 (HadISST1; Rayner et al., 2003) and version 2 (HadISST2; Titchner and Rayner, 2014) which have a horizontal resolution of one degree. We analyzed the SIC data during 1958-2020 for the HadISST1 and 1958-2019 for the HadISST2 to compare with the SPEAR simulations described below. Since the HadISST1 covers a slightly longer period than the HadISST2, we used the SIC data from the HadISST1 to perform a persistence decadal retrospective forecast in which the observed SIC anomaly for each year of 1961-2011 is assumed to persist over the next 10 years.

It should be noted that the HadISST2 provides more consistent sea ice record than the HadISST1, because the HadISST2 employs new data sources, new bias adjustments, and new methods to estimate the sea ice concentration based on the sea ice edge information. These updates lead to higher sea ice concentration and larger extent for some regions and periods in the HadISST2 than the HadISST1 (Titchner and Rayner, 2014). Also, both the HadISST1 and HadISST2 derive the SIC data indirectly using the monthly climatology of the observations for each decade before the advent of satellite imagery in 1973. Therefore, the SIC data does not include any interannual variability before the early 1970s, but gives a general indication of sea ice variations on decadal timescales. Due to bias adjustments, the HadISST2 tends to show larger SIE after 1973 than the HadISST1 (Titchner and Rayner, 2014). Since there is a large uncertainty in the SIC data before the satellite period (Hobbs et al., 2016), we discuss physical processes underlying the multidecadal sea ice variability for the post-satellite (post-1973) period.

To compare the sea ice variations obtained from the HadISST1 and HadISST2 in the satellite period, we used another monthly SIC data which are recently released from the National Oceanic and Atmospheric Administration (NOAA) and the National Snow and Ice Data Center (NSIDC) (NOAA/NSIDC; Meier et al., 2021). The SIC data from the NOAA/NSIDC is based on the passive microwave data from several satellites and covers a period of 1979-2020 with a high resolution of 0.25 degree. We horizontally interpolated the high resolution SIC data onto the HadISST1 data grid. To compare the subsurface ocean conditions, we used monthly objective analyses of ocean temperature and salinity from EN4 dataset (Good et al., 2013). For all of these datasets, we calculated monthly anomalies by removing the monthly climatology and a linear trend using a least squares method.

2.2 CGCM Experiments

187   The fully coupled climate model we used in the present study is the SPEAR low

188 resolution (SPEAR_LO; Delworth et al., 2020) model. The SPEAR_LO consists of the AM4

189 atmospheric and LM4 land surface components (Zhao et al., 2018a, b) and the MOM6 ocean

190 and SIS2 sea ice components (Adcroft et al., 2019). The atmospheric component of the

191 SPEAR_LO has a horizontal resolution of approximately 100 km and 33 vertical levels with

192 the model top at 1 hPa. The ocean and sea ice components have a horizontal resolution of 1º

193 with a gradual decrease to 1/3º in the meridional direction toward the tropics. The ocean model

194 has 75 layers in the vertical which include 30 layers in the top 100 m with a finer resolution.

195 The ocean model uses a hybrid vertical coordinate which is based on a function of height in

196 the upper ocean, transitioning to isopycnal layers in the interior ocean. The depth of transition

197 to isopycnal layers is shallower in the tropics and deeper in the high latitudes (Adcroft et al.,

198 2019). More details of the SPEAR_LO are described in a paper by Delworth et al. (2020).

199   The SPEAR_LO is then partly constrained with observation and reanalysis to mimic

200 more realistic observational evolutions. Since the ocean observational data, in particular the

201 subsurface ocean, is relatively sparser than the atmosphere, we nudged the atmospheric model

202 winds and temperature in all the vertical levels to atmospheric reanalysis and the model SST

203 to observed SST in the SPEAR_LO decadal coupled initialization/reanalysis system

204 (SPEAR_LO_DCIS; X. Yang et al., 2021). The atmospheric and SST nudging approach allows

205 the model to generate realistic air-sea fluxes that subsequently drives the ocean (X. Yang et al.,

206 2021). The SPEAR_LO_DCIS covers a period of 1958-2020 and has 30 ensemble members,

207 starting from ocean, atmosphere, and sea ice conditions in the control simulation with

208 preindustrial atmospheric radiative forcing, called SPEAR large-ensemble simulation

209 (SPEAR_LES; Delworth et al., 2020), at model years 101, 121, 141, and every 20 years

210 thereafter until model year 681. In the SPEAR_LO_DCIS, we nudged the atmospheric model

211 winds and temperature in all the vertical levels toward the 6-hourly atmospheric product from

212 the Japanese 55-year Reanalysis (JRA-55; Kobayashi et al., 2015). We also nudged the model

213 SST toward the NOAA Extended Reconstructed Sea Surface Temperature version 5

214 (ERSSTv5; Huang et al., 2017) data. We applied the SST nudging within 60ºS-60ºN at a rate

215 of 240 W m^{-2} K^{-1}, which corresponds to a 10-day nudging timescale for a 50-m mixed-layer

216 depth. The strength of SST nudging is tapered linearly from 1.0 at 55ºS (55ºN) to 0.0 at 60ºS

217 (60ºN). Here we nudged the SST within 60ºS-60ºN, because the ERSSTv5 has a warm bias in

218 the polar region as compared to the satellite observation (Huang et al., 2017) and this may

219 affect the sea ice distribution and ocean circulation in the model. The SPEAR_LO_DCIS is

220 forced by the time-varying natural and anthropogenic radiative forcings which are the same as

221   in the SPEAR_LES. Here we employed a historical forcing for the period of 1958-2014,

222   whereas we adopted a projection forcing with the Shared Socioeconomic Pathway 5-8.5 (SSP5-

223   8.5) scenario (Kriegler et al., 2017; Riahi et al., 2017) afterwards. Volcanic aerosol forcing and

224   solar irradiance changes are also included in the model.

225   To examine prediction skills of the Antarctic sea ice multidecadal variability, we also

226   conducted SPEAR_LO decadal retrospective forecasts (SPEAR_LO_DRF; X. Yang et al.,

227   2021) starting every 1st January of 1961-2020 from the SPEAR_LO_DCIS. We used 20

228   members of the SPEAR_LO_DCIS as the initial conditions and integrated the model over 10

229   years with the time-varying natural (e.g., solar variability and volcanic aerosols) and

230   anthropogenic (e.g., CO2 concentration and aerosols) radiative forcings based on the

231   observations and developed in support of Coupled Model Intercomparison Project Phase 6

232   (CMIP6) Project (Eyring et al., 2016). To calculate monthly anomalies, we removed a lead-

233   time (i.e., 120 months lead) dependent climatology and linear trend from the output. For

234   example, we calculated monthly climatology and linear trend for 1 month lead prediction from

235   every January 1st of 1961-2011, then removed them from raw values to calculate the monthly

236   anomalies for 1 month lead prediction. Removing the liner trend allows us to assess the sea ice

237   prediction skills originating from natural variability. More details on the SPEAR_LO_DCIS

238   and SPEAR_LO_DRF can be seen in a paper written by X. Yang et al. (2021).

239   To gain more insight into possible impacts of atmosphere model resolutions on

240   representation of the Antarctic sea ice multidecadal variability, we compared two 1000-yr

241   control simulations forced with atmospheric composition fixed at levels of preindustrial era

242   between the SPEAR_LO model and SPEAR medium-resolution (SPEAR_MED; Delworth et

243   al., 2020) model. The SPEAR_MED model has a higher atmospheric and land resolution

244   (approximately 50 km) but has the same ocean and sea ice models with the SPEAR_LO model.

245   Details on the differences in simulation of the Southern Ocean multidecadal variability between

246   the two models are given in a recent paper by Zhang et al. (2022a).

247   We estimated the strength of Southern Ocean deep convection (DCV) by the maximum

248   absolute value of meridional overturning streamfunction south of 60ºS (Zhang et al., 2019) to

249   explore a possible role of Southern Ocean deep convection in the sea ice variability. We also

250   defined the mixed-layer depth at which the ocean density increases by 0.03 kg m^{-3} from its

251   value at the ocean surface. Furthermore, we evaluated the upper ocean heat balance using the

252   model output stored at each model grid. In the SPEAR model, the total ocean heat tendency

253   was calculated by a sum of horizontal advection, vertical advection, parameterized mesoscale

254   diffusion and dianeutral mixing, and surface heat fluxes.

255

3. Results

3.1 Antarctic Sea Ice Multidecadal Variability Simulated in SPEAR_LO Model

256

257

258 We show in Fig. 1 the annual mean SIC from the HadISST1 and the SPEAR_LO_DCIS. The

259 observation (Fig. 1a) shows high SIC above 70 % in the Pacific and Atlantic sectors during

260 1958-2020. The SPEAR_LO_DCIS (Fig. 1b) captures the high SIC in these two regions,

261 although the simulated SIC is somewhat lower than the observed SIC. Since the monthly

262 climatology of the Antarctic SIE during austral summer for the SPEAR_LO_DCIS

263 (Supplementary Fig. S1) is lower than that for the HadISST1, the underestimation of the annual

264 mean SIC in the SPEAR_LO model is mostly due to that of the summertime SIC, which is also

265 reported in other CGCMs contributing to the CMIP6 (Roach et al., 2020). We find a similar

266 pattern for the satellite period of 1979-2020, although the monthly climatology of the Antarctic

267 SIC during austral winter for the SPEAR_LO_DCIS is higher than that for the NOAA/NSIDC

268 (Supplementary Fig. S1; see also Bushuk et al., 2021).

269 Standard deviation of 5-yr running mean SIC anomalies from the observation (Fig. 1c)

270 shows a large sea ice variability near the edge of sea ice in the Pacific sector and also near the

271 coastal region of the eastern Weddell Sea. Here we employed a 5-yr moving average of the

272 monthly SIC anomalies to extract low-frequency variability beyond a decade. The large sea ice

273 variability near the edge of sea ice in the Pacific sector is mostly due to that during austral

274 autumn-spring (Supplementary Figs. S2c, e, g), while the large sea ice variability in the coastal

275 region of the eastern Weddell Sea is attributed to that during austral spring-autumn

276 (Supplementary Figs. S2a, c, g). This represents seasonal differences in the decadal sea ice

277 variability over different regions. The SPEAR_LO_DCIS (Fig. 1d) also exhibits a large sea ice

278 variability in these two regions, but the simulated SIC variability is much larger in the Weddell

279 Sea. This is mostly due to the larger SIC variability simulated in the eastern Weddell Sea during

280 austral winter and spring (Supplementary Figs. S2f, h), although the SPEAR_LO_DCIS tends

281 to capture the observed SIC variability there during austral summer and autumn

282 (Supplementary Figs. S2b, d).

283 In the coastal region of the eastern Weddell Sea, successive polynya events occurred

284 during austral winter of 1974-1976 (Carsey, 1980). The Weddell polynya are generated through

285 various processes (Morales Maqueda et al., 2004) such as upwelling of deep warm water as a

286 result of salinity-driven vertical convection (Martinson et al., 1981) and wind-driven sea ice

287 divergence (Goosse and Fichefet, 2001). Two polynya events are recently reported during

288 2016-2017, partly contributing to the record-low sea ice in the Weddell Sea (Turner et al.,
289 2020). A weaker ocean stratification and increased ocean eddy activities are suggested to
290 provide favorable conditions for these polynya events (Cheon and Gordon, 2019), although the
291 synoptic atmospheric variability such as polar cyclones and atmospheric rivers may trigger
292 these events (Francis et al., 2019, 2020). We find that the SPEAR_LO_DCIS does not
293 overestimate the SIE decrease associated with these polynya events during 1974-1976 and
294 2016-2017 (Supplementary Fig. S3). There are other reasons for the large sea ice variation in
295 the eastern Weddell Sea of the SPEAR_LO_DCIS, which will be discussed later.

296   Time series of the pan-Antarctic SIE anomalies from the observation (Fig. 2a) show a
297 multidecadal variability with a low sea ice state (late 1970s-1990s) and a high sea ice state
298 (2000s-early 2010s). A high sea ice state before the early 1970s is also reported in several
299 studies using the satellite images of Nimbus 1 and 2 in the 1960s (Meier et al., 2013; Gagne et
300 al., 2015), the past 200-yr sea ice edge latitude data reconstructed by ice core and fast-ice
301 records (J. Yang et al., 2021), and a century-long SIE data reconstructed by major climate
302 indices (Fogt et al., 2022). However, there is a large degree of uncertainty in the sea ice data
303 before the satellite period. The SPEAR_LO_DCIS exhibits a similar multidecadal variability
304 and has a significantly high correlation (0.72) with the observed SIE anomalies from the
305 HadISST1. Here we used 12 degrees of freedom to evaluate the statistical significance for the
306 correlation coefficient, because we applied a 5-yr running mean filter to 63-yr long data. The
307 model overestimates negative SIE anomalies between the late 1970s and early 1980s (Fig. 2a).
308 This is mostly due to the model overestimation of negative SIE anomalies in the Weddell Sea
309 (Fig. 2b), and the correlation value with the HadISST1 is statistically significant (0.63), slightly
310 lower than that for the pan-Antarctic SIE. This can also be inferred from the model bias in
311 capturing the large SIC variability in the Weddell Sea (Fig. 1d). Since the ensemble spreads of
312 the negative SIE anomalies are large, some members (5 out of 30 members) in the
313 SPEAR_LO_DCIS are found to produce more reasonable SIE anomalies over the pan-
314 Antarctic and Weddell Sea as in the observation (Fig. 2a-b). The ensemble spreads seem to
315 decrease after the late 1990s when the sea ice starts to increase (Fig. 2b). This may be related
316 to different processes controlling the ensemble spreads of the SIE anomalies before and after
317 the 1990s, which will also be discussed later. Other Antarctic seas such as the Ross and
318 Amundsen-Bellingshausen Seas also show a good agreement of the SIE anomalies between the
319 HadISST1 and the SPEAR_LO_DCIS with significant correlations of 0.50 and 0.84,
320 respectively (Fig. 2c-d). It should be noted that the HadISST1 shows larger positive SIE
321 anomalies in the Amundsen-Bellingshausen Seas after 2010 than the NOAA/NSIDC (Fig. 2d),

322 probably because the HadISST1 does not use passive microwave derived sea ice concentration

323 that includes open water areas poleward of the marginal ice zone particularly in austral summer

324 (Rayner et al., 2003).

325   To explore physical mechanisms underlying the Antarctic sea ice multidecadal

326 variability in the SPEAR_LO_DCIS, we focus on the Weddell Sea which contributes the most

327 to the total sea ice variability in the SPEAR_LO_DCIS (Fig. 2a-b). Time series of 5-yr running

328 mean wind stress and curl anomalies (Fig. 3a) exhibit that a significant SIE decrease between

329 the late 1970s and early 1980s is associated with stronger westerly winds and negative wind

330 stress curl anomalies. These surface wind anomalies tend to induce anomalous upwelling of

331 warm water from the subsurface ocean on decadal and longer timescales (Ferreira et al., 2015),

332 contributing to the sea ice decrease. The westerly and negative curl anomalies coincide with a

333 positive phase of the SAM (Fig. 3b), although ensemble spreads of the SAM index (Gong and

334 Wang, 1999) are large. The IPO index (Fig. 3b), which is defined as the 13-yr running mean

335 of the SST tripole index in the tropics and subtropics (Henley et al., 2015), is negative around

336 1975 when the westerly and negative curl anomalies start to appear, but turns to positive values

337 after 1980. This out-of-phase relationship indicates that the surface wind variability in the

338 Weddell Sea is more related to the SAM than the IPO. On the other hand, the net surface heat

339 flux (Fig. 3c) shows negative (upward) anomalies between the late 1970s and early 1980s. As

340 a result of the decrease in sea ice, more heat is released from the ocean surface. We obtain an

341 opposite but similar process for the high sea ice state after the 2000s when weaker westerly

342 winds and positive curl anomalies appear. The wind stress and curl anomalies are found to have

343 almost the same amplitude as those in the low sea ice period. This implies that the surface wind

344 variability cannot fully explain the large negative SIE anomalies in the SPEAR_LO_DCIS

345 during the late 1970s and the early 1980s. This motivates us to further investigate roles of

346 surface and subsurface ocean variability in the Weddell Sea and their mechanisms.

347   The substantial SIE decrease between the late 1970s and the early 1980s is associated

348 with positive SST anomalies (Fig. 3d). A positive peak of the SST anomalies in the early 1980s

349 is preceded by positive peaks of the mixed layer depth and deep convection anomalies. Since

350 a positive peak of the deep convection anomalies leads that of mixed-layer depth anomalies by

351 a few years, the stronger deep convection deepens the mixed layer and entrains more warm

352 water from the subsurface ocean. This plays a crucial role in the development of extremely low

353 sea ice in the Weddell Sea. Moreover, the negative SIE anomalies are accompanied by positive

354 sea surface salinity (SSS) anomalies (Fig. 3e). Net salt flux into the ocean at the surface

355 associated with sea ice formation shows positive anomalies, but the amplitude is much smaller

356   than positive anomalies of the precipitation minus evaporation corresponding to net surface

357   water flux into the ocean. As a result of the decrease in sea ice, more freshwater goes into the

358   ocean, but it cannot explain the SSS increase in the Weddell Sea. Rather, the SSS increase is

359   driven by other oceanic processes, that is, the stronger deep convection and the associated

360   deeper mixed layer that entrains relatively high salinity water from the subsurface ocean.

361   To underscore the importance of subsurface ocean variability, we describe time series

362   of ocean temperature and salinity anomalies averaged in the Weddell Sea as a function of depth

363   (Fig. 4). Observation data (Fig. 4a) shows that sea ice decrease between the late 1970s and

364   early 1980s is accompanied by positive temperature anomalies in the upper 100 m and negative

365   temperature anomalies below 100 m. The SPEAR_LO_DCIS (Fig. 4b) captures a dipole

366   structure of the positive and negative temperature anomalies in the vertical, although the

367   amplitude is much larger than that in the observation. Interestingly, both the observation and

368   SPEAR_LO_DCIS (Fig. 4a-b) show that the positive temperature anomalies in the upper 100

369   m start to appear in the early 1970s, which is preceded by positive temperature anomalies below

370   100 m in the 1960s. The anomalous heat buildup in the subsurface ocean during the 1960s may

371   have links to the subsequent surface warming in the 1970s. On the other hand, the salinity

372   anomalies between the late 1970s and the early 1980s are positive in the upper 100 m and

373   negative below 200 m for both the observation (Fig. 4c) and SPEAR_LO_DCIS (Fig. 4d).

374   Since both the temperature and salinity anomalies exhibit the dipole structure in the vertical,

375   vertical ocean processes are expected to operate for inducing these anomalies.

376   The observed ocean density shows positive anomalies from the surface to the deeper

377   ocean around 1980 (Fig. 5a). The SPEAR_LO_DCIS also shows the higher density around

378   1980, although the amplitude is larger than the observation (Fig. 5b). Associated with the

379   positive density anomalies, the mixed layer anomalously deepens. The observed ocean

380   stratification, which is estimated by squared Brunt Väisälä frequency, shows negative

381   anomalies below 100 m around 1980. (Fig. 5c). The SPEAR_LO_DCIS also shows weaker

382   stratification (Fig. 5d), which starts to appear below 100 m in the 1960s and provides favorable

383   conditions for deepening of the mixed layer after the 1970s. We decomposed the density

384   anomalies into the anomalies solely dependent on temperature anomalies and other ones

385   accompanied by salinity anomalies. We find that the positive density anomalies below 100 m

386   between the late 1970s and the early 1980s are attributed to those induced by the negative

387   temperature anomalies (Figs. 4b, 5e), whereas the positive density anomalies in the upper 100

388   m arise from those associated with the positive salinity anomalies (Figs. 4d, 5f). Furthermore,

389   the negative density anomalies below 200 m in the 1960s are driven by the warm temperature

390   anomalies (Figs. 4b, 5e). Therefore, the anomalous heat buildup in the subsurface ocean during

391   the 1960s and early 1970s is responsible for the initiation of deep convection and the deepening

392   of the mixed-layer that results in warmer SST and sea ice decrease between the late 1970s and

393   the early 1980s.

394   To further investigate how the surface and subsurface ocean temperature anomalies are

395   generated, we evaluated ocean heat balance in the upper 100 m and in the subsurface 200-1200

396   m, respectively (Fig. 6). Here we combine both contributions from the dianeutral mixing and

397   mesoscale diffusion into one term, because the contribution from the mesoscale diffusion is

398   found to be much smaller than that from the dianeutral mixing. Tendency anomalies of ocean

399   temperature in the upper 100 m (Fig. 6a) are positive in the 1970s when the positive SST and

400   negative SIE anomalies (Fig. 3d) start to evolve. Net surface heat flux positively contributes to

401   the temperature tendency anomalies in the early 1970s, but shows large negative contribution

402   afterwards. Also, ocean mixing and vertical advection more positively contribute to the

403   temperature tendency anomalies in the 1970s. This indicates that the deepening of mixed layer

404   (Fig. 3d) facilitates dianeutral mixing due to weaker stratification (Fig. 5b) and entrain more

405   warm water from below the mixed layer to increase the ocean temperature at surface. We obtain

406   a similar but opposite process for negative temperature tendency anomalies after the 1990s

407   when the positive SIE anomalies start to appear (Fig. 3d). On the other hand, the heat balance

408   in the subsurface 200-1200 m (Fig. 6b) shows that positive temperature tendency anomalies in

409   the 1960s when the anomalous heat builds up in the subsurface ocean are mostly due to both

410   contributions from the horizontal advection and dianeutral mixing. This suggests that more

411   warm water is advected into the Weddell Sea from the north and the associated weakening of

412   the upper ocean stratification (Fig. 5d) helps redistribute anomalous heat in the vertical. The

413   temperature tendency anomalies turn to negative values between the 1970s and the early 1980s

414   and back to positive values after the late 1980s. Vertical advection also positively contributes

415   to the temperature tendency anomalies in early 1990s, but gradually decays and is

416   overwhelmed by the horizontal advection and dianeutral mixing. The horizontal advection and

417   dianeutral mixing appear to be more important for the subsurface ocean temperature variability.

418   We have so far discussed physical processes for ensemble mean fields of the

419   SPEAR_LO_DCIS, but this analysis does not provide any explanation for the ensemble

420   spreads representing model uncertainty. To explore the underlying causes of ensemble spreads

421   in a simple way, we performed inter-member correlation analysis for 30 ensemble members of

422   the SPEAR_LO_DCIS. Here we calculated the correlation between the anomalies of SIE and

423   other variables simulated from the 30 ensemble members, assuming that initial differences in

424 the anomalies of other variables lead to those in the SIE anomalies. Figure 7a shows time series

425 of inter-member correlation coefficients between the 5-yr running mean SIE anomalies and the

426 leading zonal wind stress anomalies in the Weddell Sea as a function of lead years. Zonal wind

427 stress anomalies have significantly large negative correlations with SIE anomalies by 3-4 lead

428 years during the 1970s and the 1980s when the sea ice anomalously decreases. This means that

429 ensemble members with stronger westerly winds than the ensemble mean tend to simulate

430 larger sea ice decrease 3-4 years later. The negative correlations become stronger with longer

431 lead times after the late 1990s when the sea ice anomalously increases. This represents more

432 influence of weaker westerly winds on the anomalous sea ice increase. We obtain similar but

433 opposite correlations between the SIE anomalies and the leading wind stress curl anomalies

434 (Fig. 7b). Ensemble members with more negative curl anomalies than the ensemble mean tend

435 to simulate larger sea ice decrease in the 1970s and the 1980s, and vice versa after the late

436 1990s.

437 Inter-member correlations between the SIE anomalies and the leading MLD anomalies

438 (Fig. 7c) show significantly large and negative values by 3-4 lead years in the 1970s and the

439 1980s and by 5-6 lead years after the late 1990s. This indicates that ensemble members with

440 deeper mixed layer than the ensemble mean tend to simulate larger sea ice decrease 3-4 years

441 later in the 1970s and the 1980s, whereas the members with shallower mixed layer than the

442 ensemble mean tend to simulate larger sea ice increase 5-6 years later after the late 1990s. It

443 should be noted that we used spatially averaged values over the whole Weddell Sea, so the

444 results also include the destratified process near the coast dominated by sea ice production.

445 However, the SIE variability in the Weddell Sea is pronounced in the open water (Fig. 1d), so

446 the results mostly represent the open-water stratified process of cold/fresh water over

447 warm/salty circumpolar deep water. Similarly, we find negative correlations between the SIE

448 anomalies and the leading deep convection anomalies (Fig. 7d), but the links with the deep

449 convection become weaker after the late 1990s. This is partly due to the definition of deep

450 convection estimated over the entire Southern Ocean, but this has further implication that the

451 deep convection becomes weaker after the late 1990s and it cannot strongly influence the upper

452 ocean temperature below sea ice. This may be responsible for smaller ensemble spreads of the

453 SIE anomalies in the Weddell Sea after the late 1990s when the sea ice starts to increase (Fig.

454 2b). Therefore, the large uncertainty in the simulated amplitude of Southern Ocean deep

455 convection contributes more to that in the sea ice decrease in the late 1970s and 1980s, while

456 the model uncertainty in the surface wind variability contributes more to that in sea ice increase

457 after the late 1990s (Fig. 7a-c). This result is consistent with negative contributions from the

458 dianeutral mixing and vertical advection to the upper 100-m ocean temperature (Fig. 6a), which

459 is associated with shallower mixed layer after the 1990s (Fig. 3d) and weakening of westerly

460 winds after the 2000s (Fig. 3a).

461

3.2 Skillful Prediction of Antarctic Sea Ice Multidecadal Variability

463   For quantitative assessment of prediction skills of the Antarctic sea ice multidecadal

464 variability, we calculated anomaly correlations (ACCs) between the 5-yr mean observed SIC

465 anomalies from the HadISST1 and the 5-yr mean predicted SIC anomalies from 20 ensemble

466 members of the SPEAR_LO_DRF for each lead time of 1-5 years and 6-10 years (Fig. 8). Here

467 we used 50 degrees of freedom to evaluate statistical significance of the ACC, because we

468 performed decadal reforecasts independently starting from each year of 1961-2011. Persistence

469 prediction using the observed SIC anomalies shows very limited prediction skills of the sea ice

470 variability in the Antarctic seas at a lead time of 1-5 years (Fig. 8a). The ACCs significantly

471 drop below zero at a lead time of 6-10 years (Fig. 8b), indicating that the observed SIC

472 anomalies cannot persist beyond five years. This can also be seen in the year-to-year ACCs

473 (Supplementary Fig. S4) that shows the highest values in lead year 1, quickly decay in lead

474 year 2, then vanish afterward.

475   The ACCs in the SPEAR_LO_DRF are significantly high at a lead time of 1-5 years

476 (Fig. 8c), as compared to the persistence prediction (Fig. 8a). In particular, the ACCs become

477 higher in the Amundsen-Bellingshausen Seas, Weddell Sea, and Indian sector. These regions

478 well correspond to those with higher ACCs of the SST in the model (see Fig. 10 in X. Yang et

479 al., 2021), indicating a close relationship between the SIC and SST variations. The ACCs in

480 these regions become smaller but remain significant for a lead time of 6-10 years (Fig. 8d). The

481 high ACCs at a lead time of 1-5 years are mostly due to those during austral autumn-spring

482 (Supplementary Figs. S5c, e, g), while the significant ACCs at a lead time of 6-10 years are

483 mainly attributed to those during austral winter and spring (Supplementary Figs. 5f, h). Decadal

484 sea ice predictability during austral summer (Supplementary Figs. S5a, b) is the lowest, because

485 the sea ice extent reaches its minimum and the decadal SIC variability is confined near the

486 Antarctic coast occupying smaller areas (Supplementary Fig. S2a). We can also find that the

487 year-to-year prediction skills of the ACC from the SPEAR_LO_DRF (Supplementary Fig. S6)

488 are higher than those from the persistence prediction (Supplementary Fig. S4), although the

489 amplitude of the ACC (Supplementary Fig. S6) is lower than the prediction skills of 5-yr mean

490 SIC (Fig. 8c-d) probably due to large interannual variations of the Antarctic SIC. The

491   SPEAR_LO_DRF has significant skills in predicting the low-frequency sea ice variability in

492   the Antarctic seas.

493   To further demonstrate the spatio-temporal evolution of prediction skills in the

494   SPEAR_LO_DRF, we calculated the ACCs of the 5-yr mean SIC anomalies in the pan-

495   Antarctic region and the Weddell Sea as a function of lead times (Fig. 9a-b). The ACCs of the

496   pan-Antarctic SIC anomalies in the SPEAR_LO_DRF are significantly higher than those in

497   the persistence prediction for any lead times from 1-5 years to 6-10 years (Fig. 9a). A few

498   ensemble members have low ACCs comparable to the persistence prediction, but the ACCs of

499   the ensemble mean SIC anomalies are high at around 0.4-0.6. We obtain similar results for the

500   ACCs of the SIC anomalies in the Weddell Sea (Fig. 9b), but the ACCs become insignificant

501   after a lead time of 6-10 years. Overall, the ACCs in the Weddell Sea are lower than those in

502   the pan-Antarctic region.

503   Since the ACCs do not evaluate skills for the amplitude of the predicted anomalies, we

504   calculated time series of the 5-yr running mean SIC anomalies in the pan-Antarctic region and

505   the Weddell Sea for different lead times from 1-5 years to 6-10 years (Fig. 9c-d). The

506   SPEAR_LO_DRF well captures the observed SIC anomalies in the pan-Antarctic region (Fig.

507   9c), but the experiment with a lead time of 1-5 years overestimates the negative SIC anomalies

508   observed in the 1980s. As the lead time increases toward 6-10 years, the amplitude of negative

509   SIC anomalies predicted in the model becomes closer to that of the observed anomalies. The

510   predicted SIC anomalies return to neutral at around 2000 and become positive afterwards,

511   although the model underestimates the positive SIC anomalies observed in the early 2010s. We

512   find a similar multidecadal SIC variability in the Weddell Sea (Fig. 9d), but the observed SIC

513   anomalies largely fluctuate on a shorter timescale, so the model cannot capture positive SIC

514   anomalies in the early 1990s and negative SIC anomalies in the mid-1970s and late 1990s. This

515   motivates us to explore the predictability of the low-frequency sea ice variability focusing on

516   the pan-Antarctic region.

517   The temporal evolution of the pan-Antarctic SIC anomalies in the SPEAR_LO_DRF

518   (Fig. 10a) shows that positive and negative SIC anomalies predicted at a lead time of 1-5 years

519   tend to persist over five years up to a lead time of 6-10 years. Negative SIC anomalies predicted

520   in the 1980s for a lead time of 1-5 years gradually weaken as the lead time increases, but remain

521   to have the same sign in the late 1980s and early 1990s for a lead time of 6-10 years. The

522   negative SIC anomalies in the late 1980s and early 1990s for a lead time of 6-10 years are

523   associated with positive zonal wind anomalies and negative meridional wind anomalies (Fig.

524   10b-c). The stronger westerly acts to induce northward Ekman current anomalies on

525   interannual and shorter timescales, but on decadal and longer timescales, the associated

526   upwelling of warm water from the subsurface ocean tends to reduce the SIC (Ferreira et al.,

527   2015). Also, the northerly wind anomalies contribute to the SIC decrease by bringing more

528   warm air from the north during the period. The wind stress curl (Fig. 10d) shows positive

529   anomalies in the 1980s for a lead time of 1-5 years and also in the late 1980s and early 1990s

530   for a lead time of 6-10 years. However, the positive wind stress curl anomalies tend to weaken

531   the upwelling of warm water from the subsurface ocean and decrease the upper ocean

532   temperature. This is inconsistent with sea ice decrease during that period. The westerly

533   anomalies in the late 1980s and early 1990s for a lead time of 6-10 years are associated with a

534   positive phase of the SAM (Fig. 10e), while the IPO index changes from the positive to

535   negative values (Fig. 10f). The closer link of the surface wind variability with the SAM is

536   consistent with the previous discussion in the Weddell Sea (Fig. 3b). The net surface heat flux

537   (Fig. 10g) also shows negative anomalies in the 1980s and early 1990s for all lead times. This

538   represents more heat release from the ocean surface as a result of the sea ice decrease. We

539   obtain similar but opposite processes for the positive SIC anomalies after the 2000s.

540   To elucidate a potential role of ocean variability, we plotted temporal evolution of 5-yr

541   running mean anomalies of predicted ocean variables (Fig. 11). The Southern Ocean SST (Fig.

542   11a) shows positive anomalies in the 1980s for a lead time of 1-5 years and in the late 1980s

543   and early 1990s for a lead time of 6-10 years. This represents persistence of the predicted SST

544   anomalies over five years. The positive SST anomalies are strongly accompanied by positive

545   mixed-layer depth anomalies (Fig. 11c) and positive deep convection anomalies (Fig. 11e) in

546   the 1980s for lead times between 1-5 years and 3-7 years. As explained earlier, the stronger

547   deep convection and the associated deeper mixed layer may contribute to the positive SST

548   anomalies by entraining warm water from the subsurface ocean into the surface mixed layer.

549   During that period, SSS anomalies (Fig. 11b) are positive in association with the positive

550   anomalies of the net salt flux into the ocean (Fig. 11d). Precipitation minus evaporation

551   corresponding to the net surface water flux into the ocean (Fig. 11f) also shows negative

552   anomalies in the 1980s. This represents more evaporation from the ocean surface as a result of

553   sea ice decrease. Given that the amplitude of the freshwater flux anomalies is much larger than

554   the salt flux anomalies, the evaporation from the ocean surface contributes more to the SSS

555   increase in the 1980s. In addition to the effect of surface evaporation, the stronger deep

556   convection and deepening of the mixed layer help increase the SSS during that period. We

557   obtain similar but opposite processes for the sea ice increase after the 2000s, but the deep

558   convection anomalies remain positive until the early 2000s, which cannot explain a shallower

559   mixed layer. More freshwater input (Fig. 11f) or anomalous heat input (Fig. 10g) into the
560   surface mixed layer may contribute to the shallower mixed layer. This indicates more active
561   roles of atmosphere-ocean interaction near the surface than the deep convection variability.

562   To further examine possible links with atmosphere and ocean variability among
563   ensemble members, we calculated the temporal evolution of inter-member correlations
564   between the SIC anomalies for a lead time of 6-10 years and the SST anomalies for each lead
565   time from 1-5 years to 6-10 years (Fig. 12a). The SIC anomalies predicted at a lead time of 6-
566   10 years show significantly negative correlations with the SST anomalies in the 1980s for a
567   lead time of 1-5 years. This means that ensemble members with larger positive SST anomalies
568   in the 1980s tend to predict larger negative SIC anomalies five years later. Zonal and
569   meridional wind stress anomalies (Fig. 12b-c) show significantly negative and positive
570   correlations with the SIC anomalies, respectively, as expected from the ensemble mean results
571   (Fig. 10b-c). However, the links with the wind stress curl anomalies (Fig. 12d) are much weaker.
572   On the other hand, the mixed-layer depth and deep convection anomalies in the 1980s predicted
573   at a lead time of 1-5 years (Fig. 12e-f) show significantly negative correlations with the SIC
574   anomalies for a lead time of 6-10 years. This indicates that ensemble members with a stronger
575   deep convection and a deeper mixed layer than the ensemble mean tend to predict a larger sea
576   ice decrease five years later and vice versa. However, the links with deep convection becomes
577   weaker after the 2000s when the sea ice anomalously increases. These results suggest that
578   subsurface ocean variability contributes to skillful and long lead-time prediction of sea ice
579   decrease in the 1980s, while atmosphere-ocean interaction near the surface plays more
580   important roles in predicting sea ice increase after the 2000s.

581

4. Summary and Discussion

583   This study has examined the relative importance of the Southern Ocean deep
584   convection and surface winds in the Antarctic sea ice multidecadal variability and predictability
585   using the GFDL SPEAR_LO model. Observed SIE anomalies show a multidecadal variability
586   with a low sea ice state (late 1970s-1990s) and a high sea ice state (2000s-early 2010s). The
587   increasing SIE trend from the late 1990s to the early 2010s is reported in many studies (e.g.,
588   Yuan et al. 2017; Parkinson 2019), and this is in contrast to a significant SIE decrease in the
589   early and middle twentieth century, estimated from century-long SIE reconstructed data (Fogt
590   et al. 2022). These results suggest that a low-frequency variability beyond a decade exists in
591   the Antarctic SIE.

592   When the SPEAR_LO model is constrained with atmospheric reanalysis winds and

593   temperature and observed SST (i.e., SPEAR_LO_DCIS), the model reproduces the overall

594   observed multidecadal variability of the Antarctic SIE. The broad SIE decrease in the Southern

595   Ocean from the late 1970s to the 1990s mainly occurred in the Weddell Sea. This is driven by

596   a stronger deep convection in the Southern Ocean and the associated warming of the upper

597   ocean, which have not been well explored in previous studies on the Weddell Sea variability

598   (Venegas and Drinkwater, 2001; Hellmer et al., 2009; Murphy et al., 2014; Morioka and

599   Behera, 2021). We have also demonstrated that the Southern Ocean deep convection may play

600   a role in the skillful prediction of the Antarctic sea ice decrease from the late 1970s to the 1990s.

601   Ensemble members with stronger (weaker) deep convection than the ensemble mean tend to

602   predict deeper (shallower) mixed layer, higher (lower) SST and larger (smaller) sea ice

603   decrease in the 1980s. Our results are in good agreement with a previous study by Zhang et al.,

604   (2019). They have demonstrated that a gradual weakening of the deep convection in their

605   CGCM simulation initiated from an active phase of the deep convection is the key to a realistic

606   representation of the Southern Ocean cooling and the associated Antarctic SIE increase in

607   recent decades.

608   The SPEAR_LO_DCIS well captures the observed multidecadal variability of the

609   Antarctic SIE (Fig. 2), but overestimates the SIE decrease in the Weddell Sea around the 1980s

610   (Fig. 2b). In the 1970s, the Weddell Sea experienced three consecutive polynya events during

611   austral winters between 1974 and 1976 in observations. Strengthening of westerly winds and

612   the associated stronger deep convection bring more warm water to the surface and cause

613   significant sea ice loss in the Weddell Sea (Cheon et al., 2014, 2015). Since the model is

614   constrained with atmospheric reanalysis winds and temperature and observed SST, the

615   overestimation of the SIE decrease in the Weddell Sea is attributed to that of the deep

616   convection in the model. In fact, the simulated ocean temperature anomalies in the

617   SPEAR_LO_DCIS (Fig. 4b) are larger than the observed temperature anomalies (Fig. 4a),

618   although the observed temperature may have some uncertainty due to an insufficient number

619   of subsurface ocean observations. Consistently, ensemble members with weaker deep

620   convection than the ensemble mean tend to capture a smaller SIE decrease than that observed

621   in the Weddell Sea (Fig. 2b). Therefore, realistic simulation of the Southern Ocean deep

622   convection is the key for reproducing the Antarctic SIE decrease from the late 1970s.

623   The use of convective models may be helpful for accurate simulation and prediction of

624   the SIE decrease in the 1980s and the increasing SIE trend afterwards. For example, using a

625   'non-convective' CGCM that cannot simulate open water deep convection in the Southern

19

626   Ocean where the wintertime mixed-layer depth exceeds 2000 m (de Laverage et al., 2014),

627   Blanchard-Wrigglesworth et al. (2021) demonstrated that even with the surface winds and SST

628   initializations in the Southern Ocean, the model could not reproduce the Antarctic SIE decrease

629   in the 1980s and did not well capture the increasing SIE trend afterwards. They have suggested

630   that the results may be conditioned by the feature of the model that does not simulate the deep

631   convection in the Southern Ocean, while some of the model failure in simulating the increasing

632   sea ice trend may be due to the model biases in the sea ice drift velocity (Sun and Eisenman

633   2021). Therefore, in this study, we used the SPEAR_LO model that is classified as a

634   'convective' model (de Laverage et al., 2014) to demonstrate the role of deep convection in the

635   low-frequency sea ice variability.

636   A recent study by Zhang et al. (2022a) has reported that the SPEAR_MED model

637   (Delworth et al., 2020) with a higher atmospheric resolution tends to simulate a weaker deep

638   convection variability in the Southern Ocean than the SPEAR_LO model. The standard

639   deviation of 5-yr running mean SIC anomalies from the 1000-yr SPEAR_LO control

640   simulation (SPEAR_LO_CTL) with the preindustrial atmospheric radiative forcings (Fig. 13a)

641   is larger in the Pacific and Atlantic sectors than that from the SPEAR_MED control simulation

642   (SPEAR_MED_CTL; Fig. 13b). This makes the SIC variability in the SPEAR_MED_CTL

643   closer to the observed one (Fig. 1c) and appears to have links to smaller mixed-layer depth

644   variability in the SPEAR_MED_CTL (Fig. 13d) than in the SPEAR_LO_CTL (Fig. 13c). The

645   weaker deep convection variability in the SPEAR_MED_CTL appears to contribute to the

646   weaker mixed-layer variability and hence the weaker sea ice variability. Decadal reforecasts

647   using the SPEAR_MED model may demonstrate more reasonable prediction skills of the

648   Antarctic sea ice low-frequency variability than those using the SPEAR_LO model, and this is

649   our future work.

650   This study has further identified that the Southern Ocean deep convection gradually

651   weakens after the 1990s and the surface wind variability starts to play a greater role in the

652   Antarctic SIE increase after the 2000s. Weakening of the deep convection may be attributed to

653   both an internal Southern Ocean multidecadal variability (Zhang et al., 2021) and a surface

654   freshening owing to anthropogenic forcings (de Lavergne et al., 2014). On the other hand, more

655   frequent occurrence of a positive phase of the SAM tends to strengthen the westerly winds and

656   induce northward transport of cold water and sea ice, leading to the Antarctic sea ice increase

657   at a shorter timescale (e.g., J. Yang et al., 2021; Crosta, 2021). In addition, the southerly wind

658   anomalies associated with deepening of the Amundsen Sea Low assist to bring more cold air

659   from the Antarctica and enhance sea ice formation in the Ross Sea (Turner et al., 2016; Meehl

660 et al., 2016). Although the sources of decadal predictability remain unclear, skillful prediction
661 of the Antarctic SIE increase after the 2000s, which is not well reproduced in most of CMIP5
662 models (Polvani and Smith, 2013; Yang et al., 2016), requires better representation of
663 atmospheric circulation variability as well as ocean and sea ice variability in the Southern
664 Ocean (Morioka et al., 2022).

665 The Antarctic SIE has experienced a slightly increasing trend over the past decades
666 (Yuan, 2017; Parkinson, 2019). However, it has suddenly declined since 2016, reached a record
667 low in 2017, and the negative anomalies remained afterwards. Several studies attributed the
668 recent sea ice decrease to various factors including the upper Southern Ocean warming (Meehl
669 et al., 2019; Zhang et al., 2022b), the anomalous warm air advection from the north (Turner et
670 al. 2017; Wang et al. 2019), and the weakening of the midlatitude westerlies (Stuecker et al.,
671 2017; Schlosser et al., 2018; Wang et al., 2019). However, it is unclear whether the sea ice
672 decrease reflects an interannual variability or a part of low-frequency variability beyond a
673 decade, owing to a short observation record. We need to wait for this to be verified using more
674 observational data when it becomes available in the future.

675

676 **Code Availability**

677 All codes to generate the figures can be provided upon the request to the corresponding author.

678

679 **Data Availability**

680 Monthly SIC data from the HadISST1 and HadISST2 can be obtained from here:
681 https://www.metoffice.gov.uk/hadobs/hadisst/data/download.html and
682 https://www.metoffice.gov.uk/hadobs/hadisst2/data/download.html, respectively. Another
683 monthly SIC data from the NOAA/NSIDC Climate Data Record website is also available here:
684 https://nsidc.org/data/G02202/versions/4. Monthly ocean temperature and salinity data are
685 downloaded from the EN4 website: https://www.metoffice.gov.uk/hadobs/en4/download.html.

686

687 **Author Contributions**

688 Y. M. performed data analysis and wrote the first draft of the manuscript, while L. Z. provided
689 the reconstructed data and X. Y. and F. Z. performed the model experiments. All authors
690 commented on previous versions of the manuscript and approved the final manuscript.

691

692 **Competing Interests**

693   The authors declare that they have no conflict of interest.

694

Acknowledgments

702

References

703 **References**

704 Akitomo, K., Awaji, T., and Imasato, N: Open-ocean deep convection in the Weddell Sea:
705 Two-dimensional numerical experiments with a nonhydrostatic model, Deep Sea Res. Part I,
706 42, 53-73, https://doi.org/10.1016/0967-0637(94)00035-Q, 1995.

708 Adcroft, A., Anderson, W., Balaji, V., Blanton, C., Bushuk, M., Dufour, C. O., et al.: The
709 GFDL global ocean and sea ice model OM4.0: Model description and simulation features, J.
710 Adv. Mod. Ear. Sys., 11, 3167–3211, https://doi.org/10.1029/2019MS001726, 2019.

712 Blanchard-Wrigglesworth, E., Roach, L. A., Donohoe, A., and Ding, Q.: Impact of winds and
713 Southern Ocean SSTs on Antarctic sea ice trends and variability, J. Climate, 34, 949-965,
714 https://doi.org/10.1175/JCLI-D-20-0386.1, 2021.

716 Bushuk, M., Winton, M., Haumann, F. A., Delworth, T., Lu, F., Zhang, Y., Jia, L., Zhang, L.,
717 Cooke, W., Harrison, M., Hurlin, B., Johnson, N. C., Kapnick, S. B., McHugh, C., Murakami,
718 H., Rosati, A., Tseng, K., Wittenberg, A. T., Yang, X., and Zeng, F.: Seasonal Prediction and
719 Predictability of Regional Antarctic Sea Ice, J. Climate, 34, 6207-6233,
720 https://doi.org/10.1175/JCLI-D-20-0965.1, 2021.

722 Carsey, F. D.: Microwave observation of the Weddell Polynya. Mon, Wea. Rev., 108, 2032-
723 2044, https://doi.org/10.1175/1520-0493(1980)108<2032:MOOTWP>2.0.CO;2, 1980.

725 Cavalieri, D. J., Parkinson, C. L., and Vinnikov, K. Y.: 30-Year satellite record reveals
726 contrasting Arctic and Antarctic decadal sea ice variability, Geophys. Res. Lett., 30,
727 https://doi.org/10.1029/2003GL018031, 2003.

729 Cheon, W. G., Park, Y. G., Toggweiler, J. R., and Lee, S. K.: The relationship of Weddell
730 Polynya and open-ocean deep convection to the Southern Hemisphere westerlies, J. Phys.
731 Oceanogr., 44, 694-713, https://doi.org/10.1175/JPO-D-13-0112.1, 2014.

733 Cheon, W. G., Lee, S. K., Gordon, A. L., Liu, Y., Cho, C. B., and Park, J. J.: Replicating the
734 1970's Weddell polynya using a coupled ocean-sea ice model with reanalysis surface flux fields,
735 Geophys. Res. Lett., 42, 5411-5418, https://doi.org/10.1002/2015GL064364, 2015.

736

737   Cheon, W. G., and Gordon, A. L.: Open-ocean polynyas and deep convection in the Southern

738   Ocean, Sci. Rep., 9, 1-9, https://doi.org/10.1038/s41598-019-43466-2, 2019.

739

740   Crosta, X., Etourneau, J., Orme, L.C. *et al.*: Multi-decadal trends in Antarctic sea-ice extent

741   driven by ENSO–SAM over the last 2,000 years, Nat. Geosci., 14, 156–160,

742   https://doi.org/10.1038/s41561-021-00697-1, 2021.

743

744   de Lavergne, C., Palter, J. B., Galbraith, E. D., Bernardello, R., and Marinov, I.: Cessation of

745   deep convection in the open Southern Ocean under anthropogenic climate change, Nature

746   Climate Change, 4, 278-282, https://doi.org/10.1038/nclimate2132, 2014.

747

748   Delworth, T. L., Cooke, W. F., Adcroft, A., Bushuk, M., Chen, J.-H., Dunne, K. A., et al.:

749   SPEAR: The next generation GFDL modeling system for seasonal to multidecadal prediction

750   and   projection,   J.   Adv.   Mod.   Ear.   Sys.,   12,   e2019MS001895,

751   https://doi.org/10.1029/2019MS001895, 2020.

752

753   Eayrs, C., Li, X., Raphael, M. N., and Holland, D. M.: Rapid decline in Antarctic sea ice in

754   recent   years   hints   at   future   change,   Nature   Geoscience,   14,   460-464,

755   https://doi.org/10.1038/s41561-021-00768-3, 2021.

756

757   Eyring, V., Bony, S., Meehl, G. A., Senior, C. A., Stevens, B., Stouffer, R. J., and Taylor, K.

758   E.: Overview of the Coupled Model Intercomparison Project Phase 6 (CMIP6) experimental

759   design and organization, Geo. Mod. Dev., 9, 1937-1958, https://doi.org/10.5194/gmd-9-1937-

760   2016, 2016.

761

762   Ferreira, D., Marshall, J., Bitz, C. M., Solomon, S., and Plumb, A.: Antarctic Ocean and sea

763   ice response to ozone depletion: A two-time-scale problem, J. Climate, 28, 1206-1226,

764   https://doi.org/10.1175/JCLI-D-14-00313.1, 2015.

765

766   Fogt, R. L., Sleinkofer, A. M., Raphael, M. N., and Handcock, M. S.: A regime shift in seasonal

767   total Antarctic sea ice extent in the twentieth century, Nature Climate Change, 12, 54-62,

768   https://doi.org/10.1038/s41558-021-01254-9, 2022.

769

770 Francis, D., Eayrs, C., Cuesta, J., and Holland, D.: Polar cyclones at the origin of the

771 reoccurrence of the Maud Rise Polynya in austral winter 2017, J. Geophys. Res. Atmos., 124,

772 5251-5267, https://doi.org/10.1029/2019JD030618, 2019.

773

774 Francis, D., Mattingly, K. S., Temimi, M., Massom, R., and Heil, P.: On the crucial role of

775 atmospheric rivers in the two major Weddell Polynya events in 1973 and 2017 in Antarctica,

776 Sci. Adv., 6, eabc2695, https://doi: 10.1126/sciadv.abc2695, 2020.

777

778 Gagné, M. È., Gillett, N. P., and Fyfe, J. C.: Observed and simulated changes in Antarctic sea

779 ice extent over the past 50 years, Geophys. Res. Lett., 42, 90-95,

780 https://doi.org/10.1002/2014GL062231, 2015.

781

782 Gong, D., and Wang, S.: Definition of Antarctic oscillation index, Geophys. Res. Lett., 26,

783 459-462, https://doi.org/10.1029/1999GL900003, 1999.

784

785 Good, S. A., Martin, M. J., and Rayner, N. A.: EN4: Quality controlled ocean temperature and

786 salinity profiles and monthly objective analyses with uncertainty estimates, J. Geophys. Res.

787 Oce., 118, 6704– 6716, https://doi.org/10.1002/2013JC009067, 2013.

788

789 Goosse, H., and Fichefet, T.: Open-ocean convection and polynya formation in a large-scale

790 ice-ocean model, Tellus A 53, 94-111, https://doi.org/10.1034/j.1600-0870.2001.01061.x,

791 2001.

792

793 Goosse, H., and Zunz, V.: Decadal trends in the Antarctic sea ice extent ultimately controlled

794 by ice–ocean feedback, The Cryosphere 8, 453-470, https://doi.org/10.5194/tc-8-453-2014,

795 2014.

796

797 Gordon, A. L.: Deep antarctic convection west of Maud Rise, J. Phys. Oceanogr., 8, 600-612,

798 1978.

799

800 Gordon, A. L., Visbeck, M., and Comiso, J. C.: A possible link between the Weddell Polynya

801 and the Southern Annular Mode, J. Climate, 20, 2558-2571,

802 https://doi.org/10.1175/JCLI4046.1, 2007.

803

The Cryosphere

Discussions

Open Access

EGU

804   Guemas, V., Doblas-Reyes, F. J., Mogensen, K., Keeley, S., and Tang, Y.: Ensemble of sea ice

805   initial conditions for interannual climate predictions, Clim. Dyn., 43, 2813-2829,

806   https://doi.org/10.1007/s00382-014-2095-7, 2014.

807

808   Guemas, V., Chevallier, M., Déqué, M., Bellprat, O., and Doblas-Reyes, F.: Impact of sea ice

809   initialization on sea ice and atmosphere prediction skill on seasonal timescales, Geophys. Res.

810   Lett., 43, 3889-3896, https://doi.org/10.1002/2015GL066626, 2016.

811

812   Hellmer, H. H., Kauker, F., and Timmermann, R.: Weddell Sea anomalies: Excitation,

813   propagation, and possible consequences, Geophys. Res. Lett., 36, L12605,

814   https://doi.org/10.1029/2009GL038407, 2009.

815

816   Henley, B. J., Gergis, J., Karoly, D. J., Power, S., Kennedy, J., and Folland, C. K.: A tripole

817   index for the interdecadal Pacific oscillation, Clim. Dyn., 45, 3077-3090,

818   https://doi.org/10.1007/s00382-015-2525-1, 2015.

819

820   Hobbs, W. R., Massom, R., Stammerjohn, S., Reid, P., Williams, G., and Meier, W.: A review

821   of recent changes in Southern Ocean sea ice, their drivers and forcings, Global Planetary

822   Change, 143, 228-250, https://doi.org/10.1016/j.gloplacha.2016.06.008, 2016.

823

824   Holland, P. R., and Kwok, R.: Wind-driven trends in Antarctic sea-ice drift, Nat. Geo., 5, 872-

825   875, https://doi.org/10.1038/ngeo1627, 2012.

826

827   Huang, B., Thorne, P. W., Banzon, V. F., Boyer, T., Chepurin, G., Lawrimore, J. H., Menne,

828   M. J., Smith, T. M., Vose, R. S., and Zhang, H.: Extended Reconstructed Sea Surface

829   Temperature, Version 5 (ERSSTv5): Upgrades, Validations, and Intercomparisons, J. Climate,

830   30, 8179-8205, https://doi.org/10.1175/JCLI-D-16-0836.1, 2017.

831

832   Killworth, P. D.: Deep convection in the world ocean, Rev. Geophys., 21, 1-26,

833   https://doi.org/10.1029/RG021i001p00001, 1983.

834

835   Kobayashi, S., Ota, Y., Harada, Y., Ebita, A., Moriya, M., Onoda, H., *et al.*: The JRA-55

836   reanalysis: general specifications and basic characteristics, J. Meteorol. Soc. Japan. Ser. II, 93,

837   5-48, https://doi.org/10.2151/jmsj.2015-001, 2015.

The Cryosphere

Discussions

EGU

Open Access

838

839   Kriegler, E., Bauer, N., Popp, A., Humpenöder, F., Leimbach, M., Strefler, J., *et al.*: Fossil-

840   fueled development (SSP5): an energy and resource intensive scenario for the 21st century,

841   Global Env. Change, 42, 297-315, https://doi.org/10.1016/j.gloenvcha.2016.05.015, 2017.

842

843   Lecomte, O., Goosse, H., Fichefet, T., De Lavergne, C., Barthélemy, A., and Zunz, V.: Vertical

844   ocean heat redistribution sustaining sea-ice concentration trends in the Ross Sea, Nat. Comm.,

845   8, 1-8, https://doi.org/10.1038/s41467-017-00347-4, 2017.

846

847   Li, X., Holland, D. M., Gerber, E. P., and Yoo, C.: Impacts of the north and tropical Atlantic

848   Ocean   on   the   Antarctic   Peninsula   and   sea   ice,   Nature,   505,   538-542,

849   https://doi.org/10.1038/nature12945, 2014.

850

851   Marchi, S., Fichefet, T., Goosse, H., Zunz, V., Tietsche, S., Day, J. J., and Hawkins, E.:

852   Reemergence of Antarctic sea ice predictability and its link to deep ocean mixing in global

853   climate models, Clim. Dyn., 52, 2775-2797, https://doi.org/10.1007/s00382-018-4292-2, 2019.

854

855   Martinson, D. G., Killworth, P. D., and Gordon, A. L.: A convective model for the Weddell

856   Polynya,   J.   Phys.   Oceanogr.,   11,   466-488,   https://doi.org/10.1175/1520-

857   0485(1981)011<0466:ACMFTW>2.0.CO;2, 1981.

858

859   Meehl, G. A., Arblaster, J. M., Bitz, C. M., Chung, C. T., and Teng, H. Antarctic sea-ice

860   expansion between 2000 and 2014 driven by tropical Pacific decadal climate variability, Nat.

861   Geo., 9, 590-595, https://doi.org/10.1038/ngeo2751, 2016.

862

863   Meehl, G. A., Arblaster, J. M., Chung, C. T., Holland, M. M., DuVivier, A., Thompson, L., *et*

864   *al*.: Sustained ocean changes contributed to sudden Antarctic sea ice retreat in late 2016, Nat.

865   Comm., 10, 1-9, https://doi.org/10.1038/s41467-018-07865-9, 2019.

866

867   Meier, W. N., Gallaher, D., Campbell, G. G.: New estimates of Arctic and Antarctic sea ice

868   extent during September 1964 from recovered Nimbus I satellite imagery, The Cryosphere, 7,

869   699-705, https://doi.org/10.5194/tc-7-699-2013, 2013.

870

871   Meier, W. N., F. Fetterer, A. K. Windnagel, and J. S. Stewart.: NOAA/NSIDC Climate Data

872   Record of Passive Microwave Sea Ice Concentration, Version 4, Boulder, Colorado USA,

873   NSIDC: National Snow and Ice Data Center, https://doi.org/10.7265/efmz-2t65, 2021.

874

875   Morales Maqueda, M. A., Willmott, A. J., and Biggs, N. R. T.: Polynya dynamics: A review

876   of observations and modeling, Rev. Geophys., 42, https://doi.org/10.1029/2002RG000116,

877   2004.

878

879   Morioka, Y., and Behera, S. K.: Remote and local processes controlling decadal sea ice

880   variability in the Weddell Sea, J. Geophys. Res. Oce., 126, e2020JC017036,

881   https://doi.org/10.1029/2020JC017036, 2021.

882

883   Morioka, Y., Iovino, D., Masina, S., and Behera, S. K.: Role of sea-ice initialization in climate

884   predictability over the Weddell Sea, Sci. Rep., 9, 1-11, https://doi.org/10.1038/s41598-019-

885   39421-w, 2019.

886

887   Morioka, Y., Iovino, D., Cipollone, A., Masina, S., and Behera, S. K.: Summertime sea-ice

888   prediction in the Weddell Sea improved by sea-ice thickness initialization, Sci. Rep., 11, 1-13,

889   https://doi.org/10.1038/s41598-021-91042-4, 2021.

890

891   Morioka, Y., Iovino, D., Cipollone, A., Masina, S., and Behera, S. K.: Decadal Sea Ice

892   Prediction in the West Antarctic Seas with Ocean and Sea Ice Initializations, Comm. Earth

893   Env., 3, 1-10, https://doi.org/10.1038/s43247-022-00529-z, 2022.

894

895   Murphy, E. J., Clarke, A., Abram, N. J., and Turner, J.: Variability of sea-ice in the northern

896   Weddell Sea during the 20th century, J. Geophys. Res. Oce., 119, 4549–4572,

897   https://doi.org/10.1002/2013JC009511, 2014.

898

899   Orsi, A. H., Johnson, G. C., and Bullister, J. L.: Circulation, mixing, and production of

900   Antarctic Bottom Water, Prog. Oceanogr., 43, 55-109, https://doi.org/10.1016/S0079-

901   6611(99)00004-X, 1999.

902

903 Parkinson, C. L.: A 40-y record reveals gradual Antarctic sea ice increases followed by
904 decreases at rates far exceeding the rates seen in the Arctic, Proc. Nat. Aca. Sci., 116, 14414-
905 14423, https://doi.org/10.1073/pnas.1906556116, 2019.

906

907 Polvani, L. M., and Smith, K. L.: Can natural variability explain observed Antarctic sea ice
908 trends? New modeling evidence from CMIP5, Geophys. Res. Lett., 40, 3195-3199,
909 https://doi.org/10.1002/grl.50578, 2013.

910

911 Power, S., Casey, T., Folland, C., Colman, A., and Mehta, V.: Inter-decadal modulation of the
912 impact of ENSO on Australia, Clim. Dyn., 15, 319-324,
913 https://doi.org/10.1007/s003820050284, 1999.

914

915 Rayner, N. A., Parker, D. E., Horton, E. B., Folland, C. K., Alexander, L. V., Rowell, D. P.,
916 Kent, E. C., and Kaplan, A.: Global analyses of sea surface temperature, sea ice, and night
917 marine air temperature since the late nineteenth century, J. Geophys. Res., 108, 4407,
918 https://doi.org/10.1029/2002JD002670, 2003.

919

920 Riahi, K., Van Vuuren, D. P., Kriegler, E., Edmonds, J., O'neill, B. C., Fujimori, S., et al.: The
921 shared socioeconomic pathways and their energy, land use, and greenhouse gas emissions
922 implications: an overview, Global Env. Change, 42, 153-168,
923 https://doi.org/10.1016/j.gloenvcha.2016.05.009, 2017.

924

925 Roach, L. A., Dörr, J., Holmes, C. R., Massonnet, F., Blockley, E. W., Notz, D., et al.: Antarctic
926 sea ice area in CMIP6, Geophys. Res. Lett., 47, e2019GL086729,
927 https://doi.org/10.1029/2019GL086729, 2020.

928

929 Schlosser, E., Haumann, F. A., and Raphael, M. N.: Atmospheric influences on the anomalous
930 2016 Antarctic sea ice decay, The Cryosphere, 12, 1103-1119, https://doi.org/10.5194/tc-12-
931 1103-2018, 2018.

932

933 Stuecker, M. F., Bitz, C. M., and Armour, K. C.: Conditions leading to the unprecedented low
934 Antarctic sea ice extent during the 2016 austral spring season, Geophys. Res. Lett., 44, 9008-
935 9019, https://doi.org/10.1002/2017GL074691, 2017.

936

937   Sun, S., and Eisenman, I.: Observed Antarctic sea ice expansion reproduced in a climate model

938   after correcting biases in sea ice drift velocity, Nat. Comm., 12, 1-6,

939   https://doi.org/10.1038/s41467-021-21412-z, 2021.

940

941   Titchner, H. A., and Rayner, N. A.: The Met Office Hadley Centre sea ice and sea surface

942   temperature data set, version 2: 1. Sea ice concentrations, J. Geophys. Res. Atmos., 119, 2864-

943   2889, https://doi.org/10.1002/2013JD020316, 2014.

944

945   Thompson, D. W., and Wallace, J. M.: Annular modes in the extratropical circulation. Part I:

946   Month-to-month variability, J. Climate, 13, 1000-1016, https://doi.org/10.1175/1520-

947   0442(2000)013<1000:AMITEC>2.0.CO;2, 2000.

948

949   Turner, J., Hosking, J. S., Marshall, G. J., Phillips, T., and Bracegirdle, T. J.: Antarctic sea ice

950   increase consistent with intrinsic variability of the Amundsen Sea Low, Clim. Dyn., 46, 2391-

951   2402, https://doi.org/10.1007/s00382-015-2708-9, 2016.

952

953   Turner, J., Phillips, T., Marshall, G. J., Hosking, J. S., Pope, J. O., Bracegirdle, T. J., and Deb,

954   P.: Unprecedented springtime retreat of Antarctic sea ice in 2016, Geophys. Res. Lett., 44,

955   6868-6875, https://doi.org/10.1002/2017GL073656, 2017.

956

957   Turner, J., Guarino, M. V., Arnatt, J., Jena, B., Marshall, G. J., Phillips, T., et al.: Recent

958   decrease of summer sea ice in the Weddell Sea, Antarctica, Geophys. Res. Lett., 47,

959   e2020GL087127, https://doi.org/10.1029/2020GL087127, 2020.

960

961   Venegas, S. A., and Drinkwater, M. R.: Sea ice, atmosphere and upper ocean variability in the

962   Weddell Sea, Antarctica, J. Geophys. Res., 106, 16747–16765,

963   https://doi.org/10.1029/2000JC000594, 2001.

964

965   Wang, G., Hendon, H. H., Arblaster, J. M., Lim, E. P., Abhik, S., and Rensch, P.: Compounding

966   tropical and stratospheric forcing of the record low Antarctic sea-ice in 2016, Nat. Comm., 10,

967   1-9, https://doi.org/10.1038/s41467-018-07689-7, 2019.

968

The Cryosphere

Discussions

Open Access

EGU

969   Yang, C. Y., Liu, J., Hu, Y., Horton, R. M., Chen, L., and Cheng, X.: Assessment of Arctic

970   and Antarctic sea ice predictability in CMIP5 decadal hindcasts, The Cryosphere, 10, 2429-

971   2452, https://doi.org/10.5194/tc-10-2429-2016, 2016.

973   Yang, J., Xiao, C., Liu, J., Li, S., and Qin, D.: Variability of Antarctic sea ice extent over the

974   past 200 years, Sci. Bull., 66, 2394-2404, https://doi.org/10.1016/j.scib.2021.07.028, 2021.

976   Yang, X., Delworth, T. L., Zeng, F., Zhang, L., Cooke, W. F., Harrison, M. J., et al.: On the

977   development of GFDL's decadal prediction system: Initialization approaches and retrospective

978   forecast   assessment,   J.   Adv.   Mod.   Earth   Sys.,   13,   e2021MS002529,

979   https://doi.org/10.1029/2021MS002529, 2021.

981   Yuan, N., Ding, M., Ludescher, and J., Bunde, A.: Increase of the Antarctic Sea Ice Extent is

982   highly significant only in the Ross Sea. Sci, Rep., 7, 1-8, https://doi.org/10.1038/srep41096,

983   2017.

985   Yuan, X., and Martinson, D. G.: Antarctic sea ice extent variability and its global connectivity,

986   J.   Climate,   13,   1697-1717,   https://doi.org/10.1175/1520-

987   0442(2000)013<1697:ASIEVA>2.0.CO;2, 2000.

989   Zhang, L., Delworth, T. L., Cooke, W., and Yang, X.: Natural variability of Southern Ocean

990   convection as a driver of observed climate trends, Nat. Clim. Change, 9, 59-65,

991   https://doi.org/10.1038/s41558-018-0350-3, 2019.

993   Zhang, L., Delworth, T. L., Cooke, W., Goosse, H., Bushuk, M., Morioka, Y., and Yang, X:

994   The dependence of internal multidecadal variability in the Southern Ocean on the ocean

995   background mean state, J. Climate, 34, 1061-1080, https://doi.org/10.1175/JCLI-D-20-0049.1,

996   2021.

998   Zhang, L., Delworth, T. L., Kapnick, S., He, J., Cooke, W., Wittenberg, A. T., Johnson, N. C.,

999   Rosati, A., Yang, X., Lu, F., Bushuk, M., McHugh, C., Murakami, H., Zeng, F., Jia, L., Tseng,

1000 K., and Morioka, Y.: Roles of Meridional Overturning in Subpolar Southern Ocean SST

1001 Trends: Insights   from   Ensemble   Simulations,   J.   Climate,   35,   1577-1596,

1002 https://doi.org/10.1175/JCLI-D-21-0466.1, 2022a.

1003

1004   Zhang, L., Delworth, T. L., Yang, X., Zeng, F., Lu, F., Morioka, Y., and Bushuk, M.: The
1005   relative role of the subsurface Southern Ocean in driving negative Antarctic Sea ice extent
1006   anomalies in 2016–2021, Comm. Earth Env., 3, 1-9, https://doi.org/10.1038/s43247-022-
1007   00624-1, 2022b.

1008

1009

1010   Zhao, M., Golaz, J.-C., Held, I. M., Guo, H., Balaji, V., Benson, R., et al.: The GFDL global
1011   atmosphere and land model AM4.0/LM4.0: 1. Simulation characteristics with prescribed SSTs,
1012   J. Adv. Mod. Earth Sys., 10, 691–734, https://doi.org/10.1002/2017MS001208, 2018.

1013

1014   Zhao, M., Golaz, J.-C., Held, I. M., Guo, H., Balaji, V., Benson, R., et al.: The GFDL global
1015   atmosphere and land model AM4.0/LM4.0: 2. Model description, sensitivity studies, and
1016   tuning   strategies,   J.   Adv.   Mod.   Earth   Sys.,   10,   735–769,
1017   https://doi.org/10.1002/2017MS001209, 2018.

1018

1019   Zunz, V., Goosse, H., and Dubinkina, S.: Impact of the initialisation on the predictability of
1020   the Southern Ocean sea ice at interannual to multi-decadal timescales, Clim. Dyn., 44, 2267-
1021   2286, https://doi.org/10.1007/s00382-014-2344-9, 2015.

1022
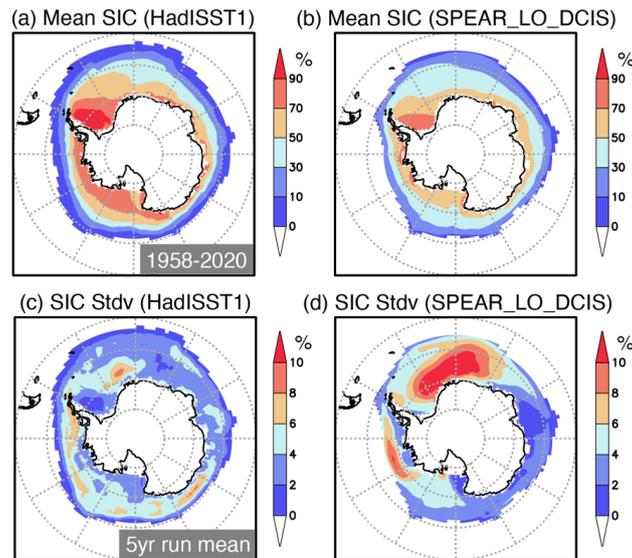
Figures

Figure 1 (a) Annual mean sea ice concentration (SIC in %) observed during 1958-2020. **(b)** Same as in **(a)**, but for the simulated SIC from the SPEAR_LO_DCIS. **(c)** Standard deviation of 5-yr running mean SIC (in %) observed during 1958-2020. **(d)** Same as in **(c)**, but for the simulated SIC from the SPEAR_LO_DCIS.
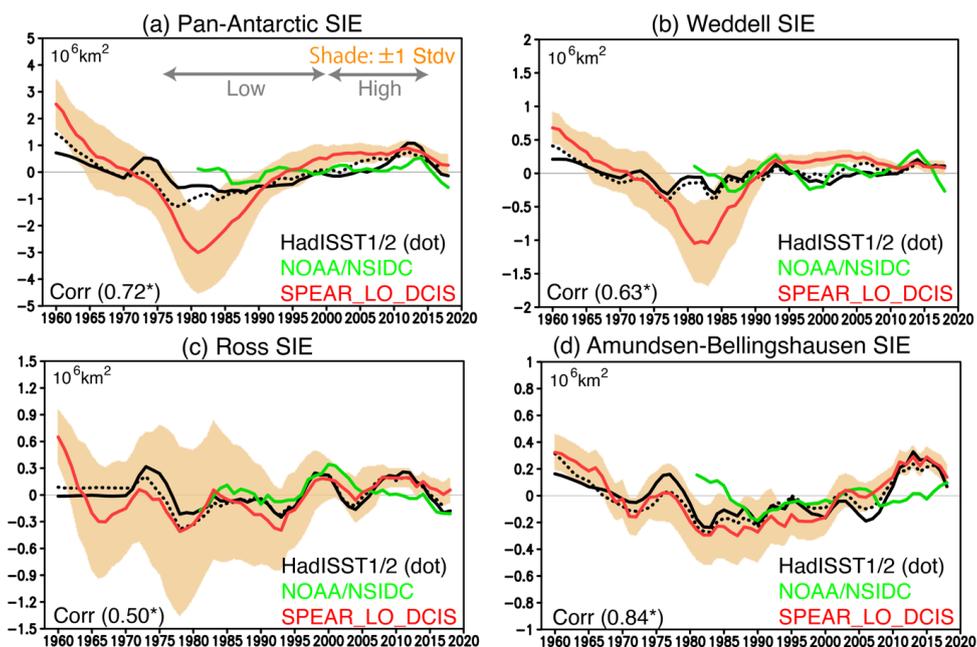
Figure 2 (a) Time series of 5-yr running mean sea ice extent (SIE in 10^6 km^2) anomalies in the pan-Antarctic region during 1958-2020. Observations from the HadISST1 (black solid line), HadISST2 (black dotted line) and the NOAA/NSIDC (green line) are shown, whereas the SPEAR_LO_DCIS is shown with a red line. Orange shades indicate one and minus one standard deviations of the SIE anomalies simulated from 30 ensemble members of SPEAR_LO_DCIS. Gray arrows correspond to a low sea ice period (late 1970s-1990s) and a high sea ice period (2000s-early 2010s). Correlation coefficient between the HadISST1 and the SPEAR_LO_DCIS is shown in the bottom left where the asterisk indicates the statistically significant correlation at 90 % confidence level using Student's *t*-test. **(b-d)** Same as in **(a)**, but for the SIE anomalies in the Weddell Sea (60º-0ºW), Ross Sea (180º-120ºW), and Amundsen-Bellingshausen Sea (120º-60ºW), respectively.
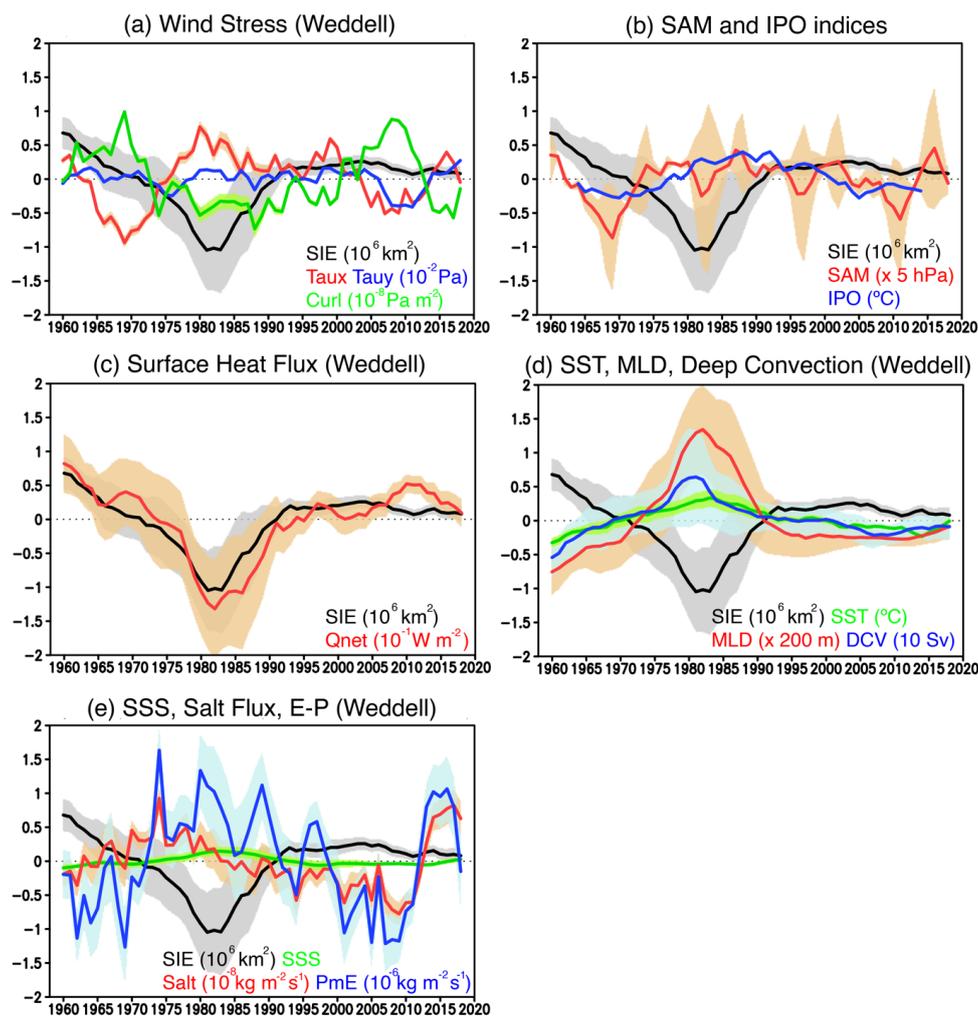
Figure 3 (a) Time series of 5-yr running mean SIE (black line in 10^6 km^2), zonal (Taux; red line in 10^{-2} Pa) and meridional (Tauy; blue line in 10^{-2} Pa) wind stress, and wind stress curl (Curl; green line in 10^{-8} Pa m^{-2}) anomalies averaged in the Weddell Sea during 1958-2020. Shades indicate one and minus one standard deviations of the anomalies from 30 ensemble members of the SPEAR_LO_DCIS. Positive wind stress curl anomalies correspond to downwelling anomalies in the ocean. **(b)** Same as in **(a)**, but for the 5-yr running mean SAM index (red line in 5 hPa) and 13-yr running mean IPO index (blue line in ℃). **(c)** Same as in **(a)**, but for the SIE (black line in 10^6 km^2) and the net surface heat flux (Qnet; red line in 10^{-1} W m^{-2}) anomalies. Positive surface heat flux anomalies correspond to more heat going into the ocean. **(d)** Same as in **(a)**, but for the SIE (black line in 10^6 km^2), sea surface temperature (SST; green line in ℃), mixed-layer depth (MLD; red line in 200 m), and deep convection (DCV;

1055   blue line in 10 Sv) anomalies. **(e)** Same as in **(a)**, but for the SIE (black line in 10^6 km^2), sea

1056   surface salinity (SSS; green line in PSU), salt flux (Salt; red line in 10^{-8} kg m^{-2} s^{-1}), and

1057   precipitation minus evaporation (PmE; blue line in 10^{-6} kg m^{-2} s^{-1}) anomalies. Positive salt flux

1058   anomalies correspond to anomalous salt going into the ocean at the surface associated with sea

1059   ice formation, whereas the positive PmE anomalies mean more freshwater going into the ocean.

1060
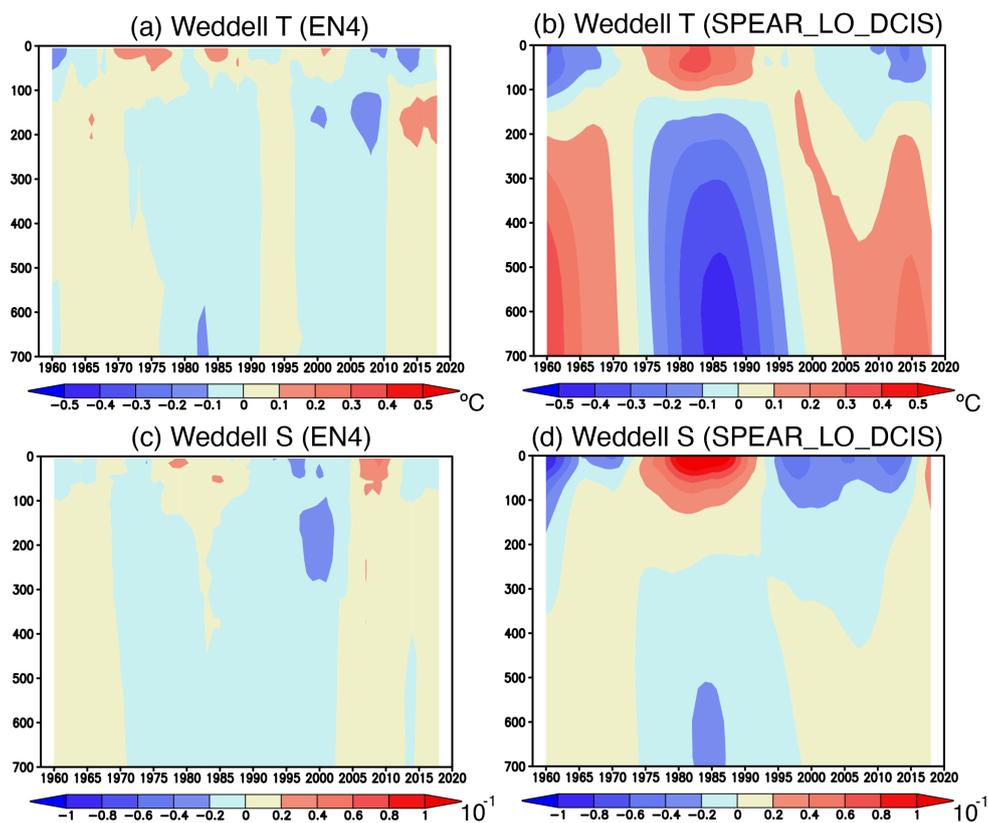
Figure 4 (a) Temporal evolution of 5-yr running mean ocean temperature (in ºC) anomalies averaged in the Weddell Sea as a function of depth (in m). **(b)** Same as in **(a)**, but for the ocean temperature anomalies simulated from the SPEAR_LO_DCIS. **(c)** Temporal evolution of ocean salinity (in 10^{-1} PSU) anomalies averaged in the Weddell Sea as a function of depth (in m). **(d)** Same as in **(a)**, but for the ocean salinity anomalies simulated from the SPEAR_LO_DCIS.
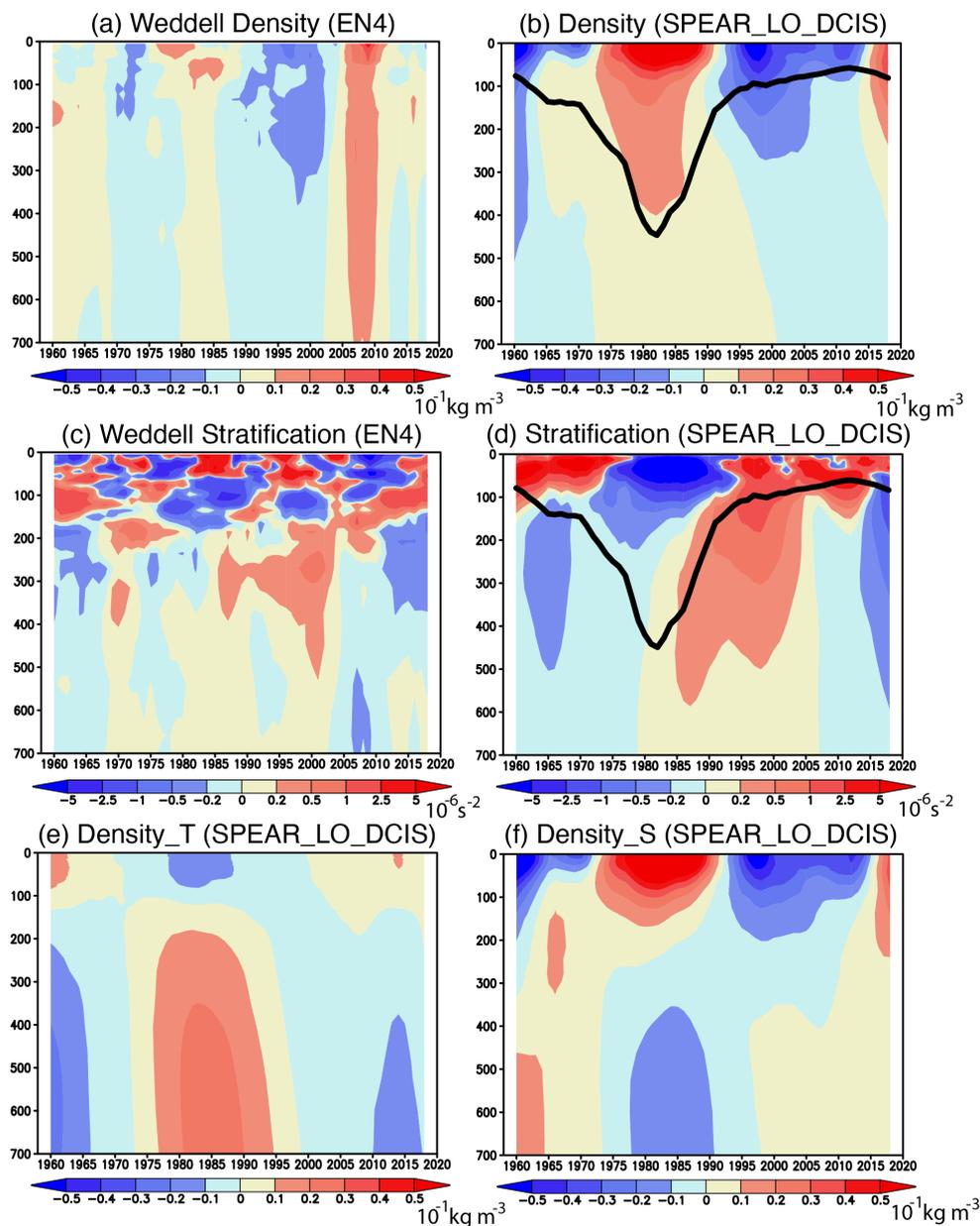
Figure 5 (a) Temporal evolution of 5-yr running mean ocean density anomalies (in 10^{-1} kg m^{-3}) averaged in the Weddell Sea from the EN4 as a function of depth (in m). **(b)** Same as in **(a)**, but for the SPEAR_LO_DCIS. A black line indicates a mixed-layer depth at which the ocean density increases by 0.03 kg m^{-3} from the one at the ocean surface. **(c)** Same as in **(a)**, but for the ocean stratification (squared Brunt-Väisälä frequency in 10^{-6} s^{-2}) anomalies. Positive stratification anomalies indicate a higher stability of sea water. **(d)** Same as in **(c)**, but for the

1076   SPEAR_LO_DCIS. A black line indicates a mixed-layer depth at which the ocean density

1077   increases by 0.03 kg m^{-3} from the one at the ocean surface. **(e)** Same as in **(b)**, but for the ocean

1078   density anomalies (in 10^{-1} kg m^{-3}) driven by the ocean temperature anomalies independent of

1079   the ocean salinity anomalies. **(f)** Same as in **(b)**, but for the ocean density anomalies (in 10^{-1} kg

1080   m^{-3}) driven by the ocean salinity anomalies independent of the ocean temperature anomalies.

1081
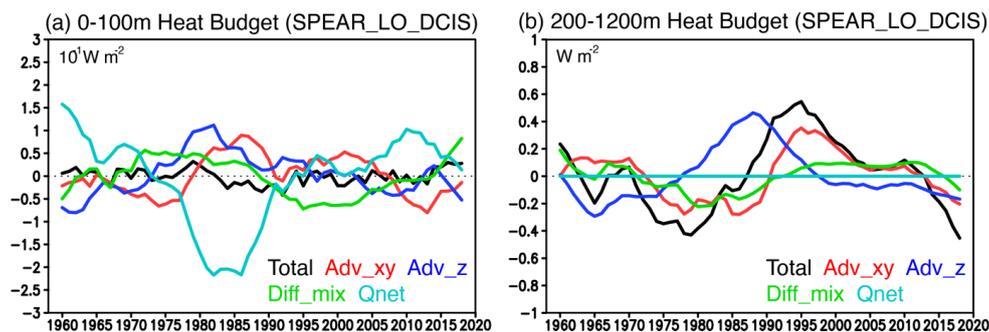
Figure 6 (a) Time series of 5-yr running mean ocean heat budget (in 10^{-1} W m^{-2}) anomalies in the upper 0-100 m of the Weddell Sea from the SPEAR_LO_DCIS. Total ocean heat tendency (Total; black line), horizontal advection (Adv_xy; red line), vertical advection (Adv_z; blue line), mesoscale diffusion and dianeutral mixing (Diff_mix; green line), and net surface heat flux (Qnet; light blue line) anomalies are shown, respectively. **(b)** Same as in **(a)**, but for the ocean heat budget (in W m^{-2}) anomalies in the upper 200-1200 m of the Weddell Sea from the SPEAR_LO_DCIS.
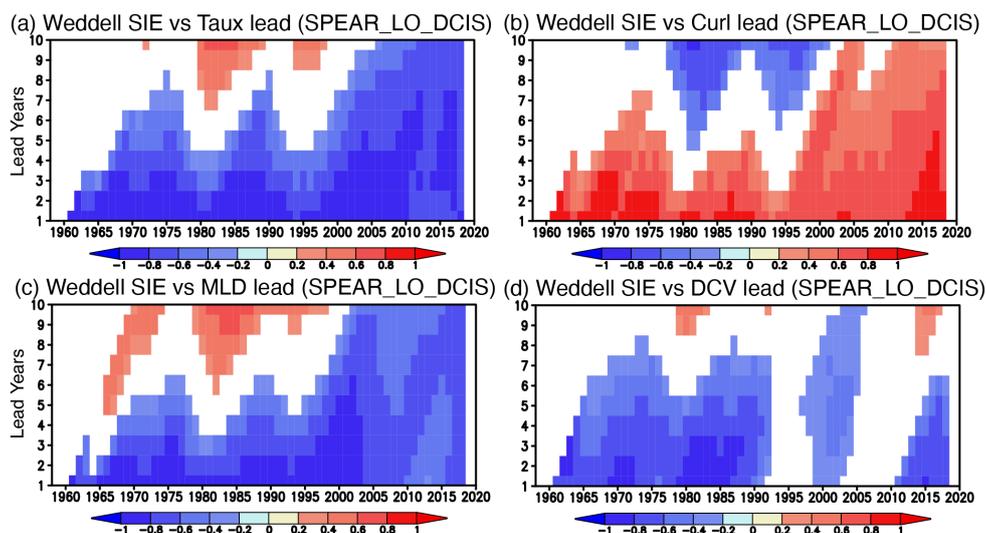
Figure 7 (a) Temporal evolution of inter-member correlation between the 5-yr running mean SIE anomalies and the 5-yr running mean zonal wind stress (Taux) averaged in the Weddell Sea from 30 ensemble members of the SPEAR_LO_DCIS as a function of lead years. Positive lead years (Y-axis) mean that the Taux anomalies lead the SIE anomalies by the number of years. Correlation coefficients that are statistically significant at 90 % using Student's t-test are shown in color. (b) Same as in (a), but for the inter-member correlation between the SIE anomalies and the wind stress curl (Curl) anomalies. (c) Same as in (a), but for the inter-member correlation between the SIE anomalies and the mixed-layer depth (MLD) anomalies. (d) Same as in (a), but for the inter-member correlation between the SIE anomalies and the deep convection (DCV) anomalies.

1103
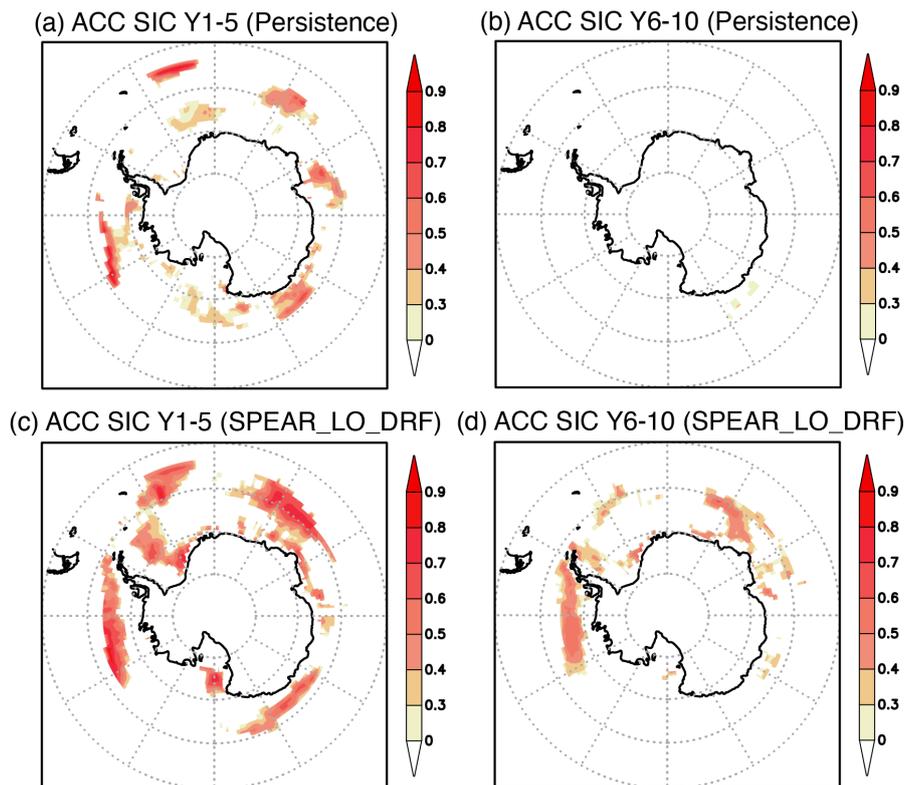
Figure 8 (a) Anomaly correlation (ACC) of the SIC anomalies from the persistence prediction at a lead time of 1-5 years. Positive ACCs that are statistically significant at 90 % using the Student's *t*-test are colored. **(b)** Same as in **(a)**, but for the ACC from the persistence prediction at a lead time of 6-10 years. **(c)** Same as in **(a)**, but for the ACC between the observed SIC anomalies and the ensemble mean SIC anomalies predicted at a lead time of 1-5 years in the SPEAR_LO_DRF. **(d)** Same as in **(c)**, but for the ACCs of the ensemble mean SIC anomalies predicted at a lead time of 6-10 years in the SPEAR_LO_DRF.

1111
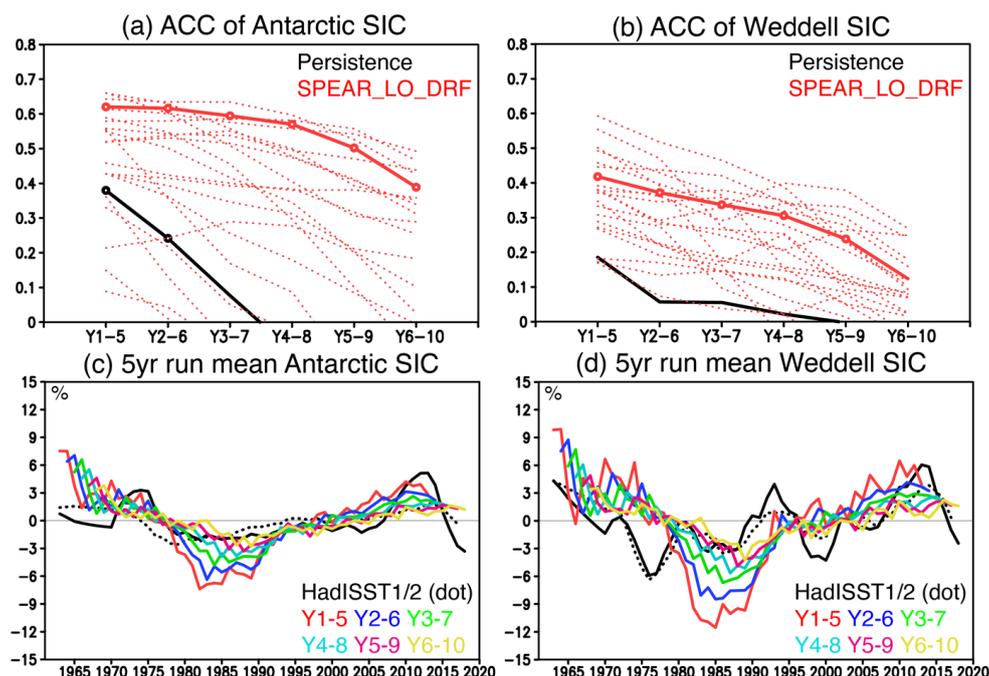
Figure 9 (a) ACCs of ensemble mean pan-Antarctic SIC anomalies predicted at lead times from 1-5 years to 6-10 years. The ACCs from the persistence prediction (black line) and the SPEAR_LO_DRF (red lines) are shown, respectively. Red dotted lines correspond to the ACCs for each of 20 ensemble members. The ACCs that are statistically significant at 90 % using Student's *t*-test are described with open circles. **(b)** Same as in **(a)**, but for the ACCs of the SIC anomalies averaged in the Weddell Sea. **(c)** Time series of 5-yr running mean pan-Antarctic SIC (in %) anomalies during 1961-2020. Black lines show the observed SIC anomalies from the HadISST1 (solid line) and HadISST2 (dotted line), whereas other colored lines correspond to the ensemble mean SIC anomalies predicted at lead times from 1-5 years to 6-10 years in the SPEAR_LO_DRF. **(d)** Same as in **(c)**, but for the SIC anomalies averaged in the Weddell Sea.
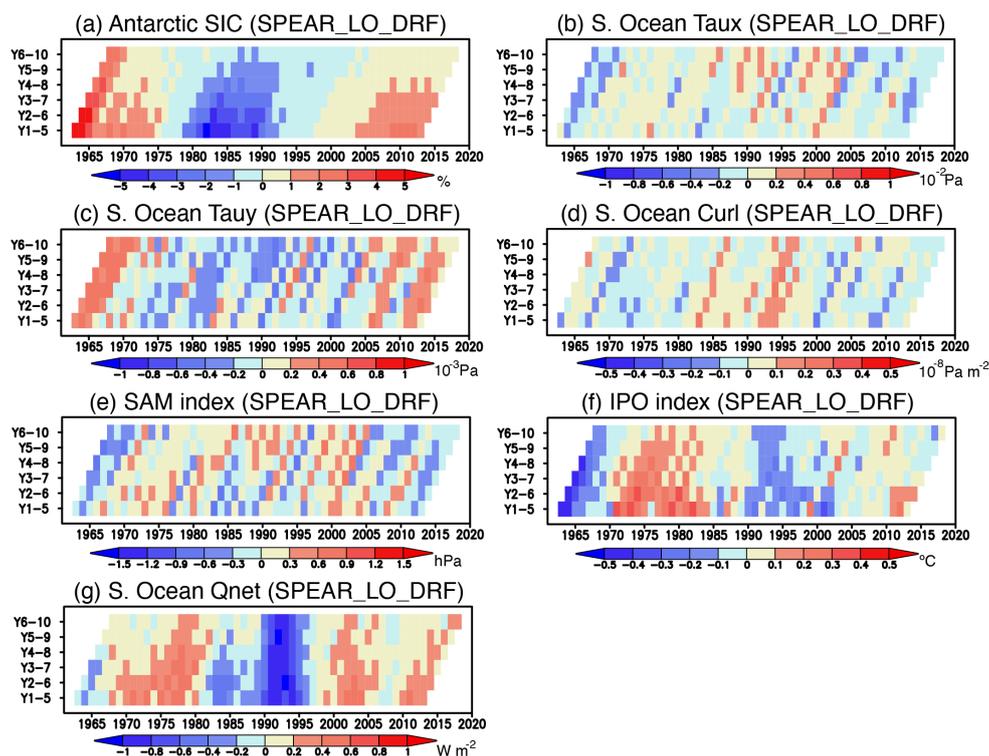
Figure 10 (a) Temporal evolution of ensemble mean pan-Antarctic SIC anomalies predicted at lead times from 1-5 years to 6-10 years in the SPEAR_LO_DRF. **(b-d)** Same as in **(a)**, but for the zonal wind stress (Taux; 10^{-2} Pa), meridional wind stress (Tauy; 10^{-3} Pa), and wind stress curl (Curl; 10^{-8} Pa m^{-2}) anomalies averaged in the Southern Ocean (south of 55°S). Positive wind stress curl anomalies correspond to downwelling anomalies in the ocean. **(e-f)** Same as in **(a)**, but for the SAM (in hPa) and IPO (in °C) indices, respectively. **(g)** Same as in **(b)**, but for the net surface heat flux anomalies (in W m^{-2}). Positive surface heat flux anomalies indicate more heat going into the ocean.
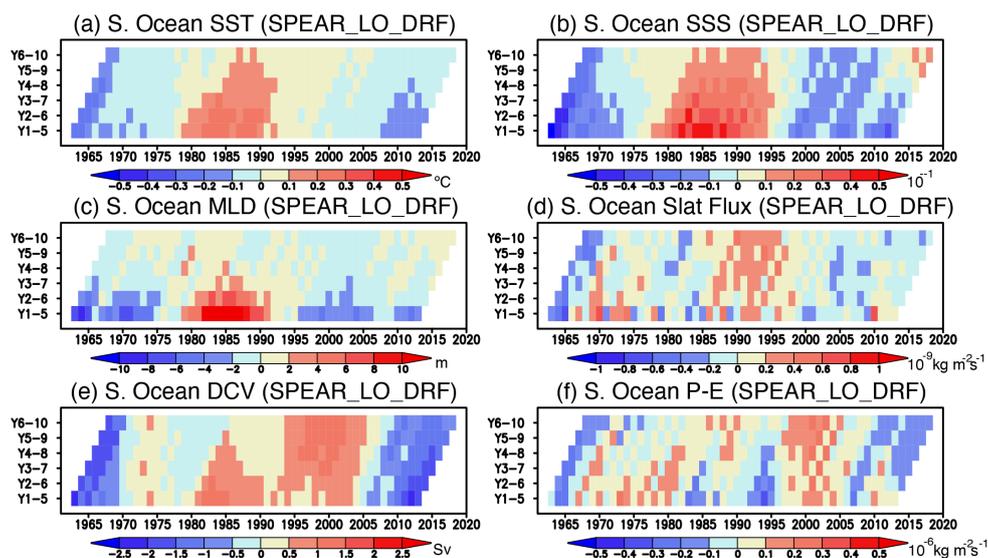
Figure 11 (a) Temporal evolution of ensemble mean Southern Ocean (south of 55ºS) SST anomalies predicted at lead times from 1-5 years to 6-10 years in the SPEAR_LO_DRF. **(b-f)** Same as in **(a)**, but for the SSS (in 10^{-1} PSU), mixed-layer depth (MLD; in m), salt flux (in 10^{-9} kg m^{-2} s^{-1}), deep convection (DCV; in Sv), and precipitation minus evaporation (P-E; in 10^{-6} kg m^{-2} s^{-1}) anomalies averaged in the Southern Ocean, respectively.
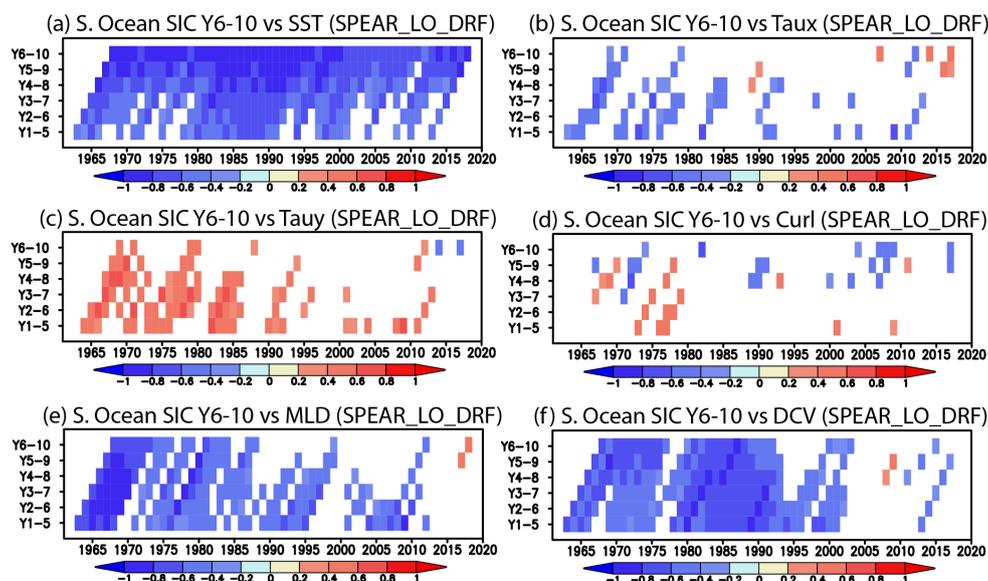
Figure 12 (a) Temporal evolution of inter-member correlation between the pan-Antarctic SIC anomalies predicted at a lead time of 6-10 years and the Southern Ocean SST anomalies predicted at lead times from 1-5 years to 6-10 years for the 20 ensemble members of the SPEAR_LO_DRF. Correlation coefficients that are statistically significant at 90 % using Student's *t*-test are colored. **(b-f)** Same as in **(a)**, but for the inter-member correlation with the zonal wind stress, meridional wind stress, wind stress curl, mixed-layer depth, and deep convection anomalies averaged in the Southern Ocean.
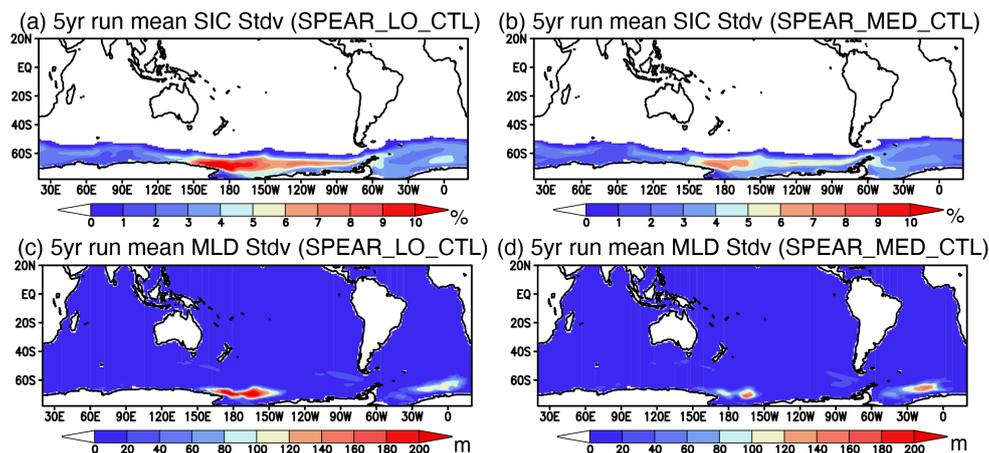
Figure 13 (a) Standard deviation of 5-yr running mean SIC (in %) anomalies from the SPEAR_LO_CTL with the preindustrial atmospheric radiative forcings. **(b)** Same as in **(a)**, but for the SPEAR_MED_CTL. **(c)** Standard deviation of 5-yr running mean mixed-layer depth (MLD, in %) anomalies from the SPEAR_LO_CTL. **(d)** Same as in **(c)**, but for the SPEAR_MED_CTL.